Department of Electronics and Nanoengineering

Characterisation of Schottky diodes and dielectric materials for millimeter wave and THz applications

Subash Khanal

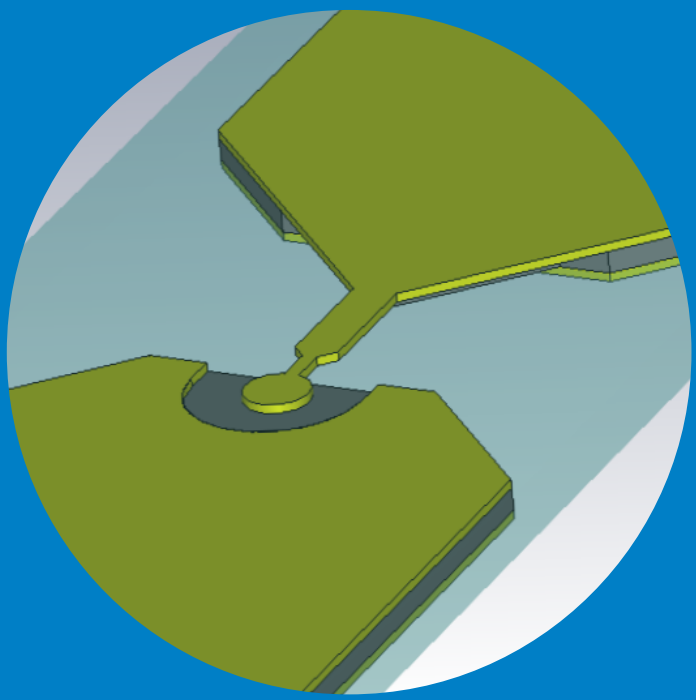

Aalto University

DOCTORAL DISSERTATIONS

Aalto University publication series
DOCTORAL DISSERTATIONS 37/2017

Characterisation of Schottky diodes and dielectric materials for millimeter wave and THz applications

Subash Khanal

A doctoral dissertation completed for the degree of Doctor of Science (Technology) to be defended, with the permission of the Aalto University School of Electrical Engineering, at a public examination held at the lecture hall AS1 (TUAS Building) on 21 March 2017 at 12 noon.

Aalto University
School of Electrical Engineering
Department of Electronics and Nanoengineering

Supervising professor
Prof. Antti V. Räisänen, Aalto University, Finland

Thesis advisors
Dr. Tero Kiuru, VTT Technical Research Centre of Finland, Finland
Dr. Juha Mallat, Aalto University, Finland

Preliminary examiners
Dr. Imran Mehdi, Jet Propulsion Laboratory, Pasadena, CA, USA
Dr. Jeffrey Hesler, Virginia Diodes Inc., Charlottesville, VA, USA

Opponent
Dr. Alain Maestrini, Observatoire de Paris - LERMA, Paris, France

Aalto University publication series
DOCTORAL DISSERTATIONS 37/2017

ISBN 978-952-60-7318-7 (printed)
ISBN 978-952-60-7317-0 (pdf)
ISSN-L 1799-4934
ISSN 1799-4934 (printed)
ISSN 1799-4942 (pdf)
http://urn.fi/URN:ISBN:978-952-60-7317-0

Unigrafia Oy
Helsinki 2017

Finland

Aalto University

Abstract

Aalto University, P.O. Box 11000, FI-00076 Aalto www.aalto.fi

Author
Subash Khanal

Name of the doctoral dissertation
Characterisation of Schottky diodes and dielectric materials for millimeter wave and THz applications

Publisher School of Electrical Engineering

Unit Department of Electronics and Nanoengineering

Series Aalto University publication series DOCTORAL DISSERTATIONS 37/2017

Field of research Radio Engineering

Manuscript submitted 17 November 2016 **Date of the defence** 21 March 2017

Permission to publish granted (date) 24 January 2017 **Language** English

☐ **Monograph** ☒ **Article dissertation** ☐ **Essay dissertation**

Abstract

This thesis work contributes to two fields of research: Schottky diode characterisation and dielectric material characterisation, both for millimeter wave and THz applications. Schottky diodes are characterised for their electrical, thermal, noise and RF properties with various measurement techniques, and an easy-to-use method is introduced for the extraction of the dielectric material properties at millimeter wave frequencies. In addition, the applications of the developed thermal characterisation method for THz Schottky diodes and of the material characterisation method are presented.

Schottky diode is a key component in almost all non-cryogenic mixer and frequency multiplier applications at 100–3000 GHz. In this work, a novel thermal characterisation method suitable for small THz Schottky diodes is introduced. This method is based on the transient current measurement and it enables the extraction of thermal resistances, thermal time-constants, and peak junction temperatures. The accuracy of the transient measurement setup is ensured with a developed verification routine and the characterization results are compared against an in-house measurement-based method and also against simulation results of two commercial 3-D thermal simulators. As an application, the developed characterisation method is applied to obtain the thermal performance of the Schottky based mixer and multiplier prototypes for the MetOp-SG satellite instruments.

Besides thermal performance, Schottky diodes are also characterised for their low-frequency noise and RF properties. Experimental investigations are carried out to study the indication of charge trapping in the THz Schottky diodes with a small anode area. Various measurement techniques are applied including I-V, capacitance and low-frequency noise measurements. Furthermore, low-barrier Schottky diodes from ACST GmbH are characterised to study their suitability for millimeter wave mixing applications because the low-barrier height enables low LO power requirement for the mixers. The performance of such diodes is evaluated, in terms of the conversion loss and the noise temperature, in a fundamental mixing configuration with measurements and simulations.

The last part of this thesis work presents the characterisation of dielectric material at millimeter wave frequencies. An easy-to-use method is introduced for the extraction of the permittivity and the loss tangent of the material sample from reflection and transmission coefficient measurements. Extraction of the material parameters are performed with two approaches. First, by using the direct comparison with the simulated S-parameter results and second, from the analytical calculations. As an application, this extraction technique is used to characterise potential substrate materials for printing millimeter wave components, e.g., antennas.

Keywords Schottky diode, thermal characterisation, dielectric material

ISBN (printed) 978-952-60-7318-7 **ISBN (pdf)** 978-952-60-7317-0

ISSN-L 1799-4934 **ISSN (printed)** 1799-4934 **ISSN (pdf)** 1799-4942

Location of publisher Helsinki **Location of printing** Helsinki **Year** 2017

Pages 127 **urn** http://urn.fi/URN:ISBN:978-952-60-7317-0

Preface

The work presented in this thesis was performed at the Department of Radio Science and Engineering of School of Electrical Engineering at Aalto University. I would like to express my gratitude to my supervisor Prof. Antti Räisänen for giving me the opportunity to work in this topic and his guidance during the thesis work. It is my privilege to have you as my supervisor. I am deeply indebted to my instructor Dr. Tero Kiuru for his enthusiastic involvement in my research and his valuable ideas, inspiring thoughts, feedback and support throughout my research career at Aalto University. I would like to thank my instructor Dr. Juha Mallat for his guidance and valuable discussions during the thesis work. I am thankful to Aalto ELEC doctoral school and European Space Agency for funding this research work. I take this opportunity to acknowledge Dr. Tapani Närhi and Dr. Petri Piironen from ESA, and Dr. Matthias Hoefle and Dr. Javier Montero from ACST GmbH for the fruitful discussions and support during the course of this research work. I am grateful to the pre-examiners Dr. Imran Mehdi and Dr. Jeffrey Hesler for their valuable comments and suggestions to improve the manuscript and Dr. Alain Maestrini for accepting to examine my thesis as an opponent.

I would like to thank all my former and current colleagues and support personnel at the department and at VTT. Thank you Krista, Arif, Jinsong, Juha A., Dimitri, Irina, Usman, Vasilii, Mazidul, Suzan, Viktor, Mirjam, Sari, Tuula, Marja, Heikki, Mikko, Hannu, and many more for helping me to walk this memorable journey. I am thankful to all the friends at Aalto University and outside for their help during all these years. Special mention to Dr. Prem Raj Adhikari, Gautam Raj Moktan, and Dr. Roshan Chudal for their continuous support, encouragement, and friendly advices on the practical aspects of life.

Finally, I express my sincere gratitude to my parents, parents-in-law,

and entire family for their blessings and love. I owe my deepest gratitude to my better half, my wife Mrs. Rashmi Dhungel for her unconditional love, support and patience during these years of my studies and always. Thank you for motivating me to accomplish these goals. This is our achievement together.

Espoo, February 23, 2017,

Subash Khanal

Contents

List of Publications

This thesis consists of an overview and of the following publications which are referred to in the text by their Roman numerals.

I S. Khanal, T. Kiuru, J. Mallat, A. V. Räisänen, and T. Närhi, "New verification routine for pulsed I-V and transient current measurement setup applied to a THz Schottky diode," *The 43rd European Microwave Conference*, Nuremberg, Germany, pp. 1279-1282, October 2013.

II S. Khanal, T. Kiuru, A. Y. Tang, M. A. Saber, J. Mallat, J. Stake, A. V. Räisänen, and T. Närhi, "Thermal characterization of THz Schottky diodes using transient current measurements," *IEEE Transactions on Terahertz Science and Technology*, vol. 4, no. 2, pp. 267-276, March 2014.

III S. Khanal, T. Kiuru, B. Thomas, J. Mallat, C. Pinta, M. Magel, A. Walber, V. Kangas, M. Perichaud, M. Brandt, T. Närhi, and A. V. Räisänen, "Characterisation of THz Schottky diodes for MetOp-SG instruments," *The 26th International Symposium on Space Terahertz Technology*, Boston, USA, March 2015.

IV S. Khanal, T. Kiuru, H. Seppä, J. Mallat, P. Piironen, and A. V. Räisänen, "Experimental investigation of traps in THz Schottky diodes," *The 9th Global Symposium on Millimeter-Waves*, Espoo, Finland, June 2016.

V S. Khanal, T. Kiuru, M. Hoefle, J. Montero, O. Cojocari, J. Mallat, P. Piironen, and A. V. Räisänen, "Characterisation of low-barrier Schottky diodes for millimeter wave mixer applications," *The 9th Global Symposium on Millimeter-Waves*, Espoo, Finland, June 2016.

VI S. Khanal, T. Kiuru, J. Mallat, O. Luukkonen, and A. V. Räisänen, "Measurement of dielectric properties at 75 - 325 GHz using a vector network analyzer and full-wave simulator," *Radio Engineering Journal: Special Issue on Advanced RF Measurement*, vol. 21, no. 2, pp. 551-556, June 2012.

VII S. Khanal, V. Semkin, V. Asadchy, J. A. Laurinaho, A. Alastalo, A. Sneck, T. Mäkelä, S. Tretyakov, and A. V. Räisänen, "Towards printed millimeter-wave components: Material characterization," *The 9th Global Symposium on Millimeter-Waves*, Espoo, Finland, June 2016.

Author's Contribution

Publication I: "New verification routine for pulsed I-V and transient current measurement setup applied to a THz Schottky diode"

This work was mainly done by the author. The measurement and publication writing was done by the author. Dr. Tero Kiuru instructed the work.

Publication II: "Thermal characterization of THz Schottky diodes using transient current measurements"

This work was mainly done by the author. The idea of the new thermal characterisation method for THz Schottky diode was formulated by the author and Dr. Tero Kiuru. Measurements, processing of measurement data and publication writing were done by the author. Mr. Mohammad Arif Saber and Dr. Aik-Yean Tang carried out the thermal simulations. Dr. Tero Kiuru and Dr. Juha Mallat instructed the work. Prof. Antti Räisänen and Dr. Tapani Närhi supervised the work.

Publication III: "Characterisation of THz Schottky diodes for MetOp-SG instruments"

This work was mainly done by the author. The simulation, measurements and publication writing were done by the author. Dr. Bertrand Thomas provided the mixer and multiplier prototypes. Dr. Tero Kiuru instructed the work.

Publication IV: "Experimental investigation of traps in THz Schottky diodes"

This is a result of collaborative work. The idea for investigation of traps in Schottky diodes was proposed by Dr. Tero Kiuru. The author performed the measurement and data processing and wrote the publication. Dr. Tero Kiuru and Dr. Heikki Seppä instructed the work. Dr. Juha Mallat and Prof. Antti Räisänen supervised the work.

Publication V: "Characterisation of low-barrier Schottky diodes for millimeter wave mixer applications"

This is a result of collaborative work. Measurements, simulations, data processing were done by the author. The idea of using fundamental mixer test jig was proposed by Dr. Tero Kiuru. Dr. Matthias Hoefle and Dr. Javier Montero provided the low-barrier diodes for the work. The author and Dr. Javier Montero jointly wrote the publication. Dr. Tero Kiuru instructed the work.

Publication VI: "Measurement of dielectric properties at 75 - 325 GHz using a vector network analyzer and full-wave simulator"

This is a result of collaborative work. The measurements, data processing, simulations and publication writing were done by the author. Dr. Olli Luukkonen developed the analytical equations for material parameter extraction. Dr. Tero Kiuru and Dr. Juha Mallat instructed the work. Prof. Antti Räisänen supervised the work.

Publication VII: "Towards printed millimeter-wave components: Material characterization"

This work was mainly done by the author. The author was responsible for measurements, simulations, data processing and writing the publication. Mr. Asko Sneck provided the polymer material samples.

List of Abbreviations

3D	Three dimensional
5G	Fifth generation
ADS	Advanced design system
AMC	Amplifier/multiplier chain
BWO	Backward wave oscillator
C-V	Capacitance-voltage
DC	Direct current
DLTS	Deep-level transient spectroscopy
DSB	Double side-band
DUT	Device under test
GaAs	Gallium arsenide
GHz	Gigahertz
GR	Generation-recombination
GSG	Ground-signal-ground
HEB	Hot electron bolometer
HFSS	High frequency structural simulator
IF	Intermediate frequency
InGaAs	Indium gallium arsenide
I-V	Current-voltage
LED	Light emitting diode
LF	Low frequency
LO	Local oscillator
MetOp-SG	Meteorological operational satellite program - second generation
MUT	Material under test
NRW	Nicolson–Ross–Weir
PCB	Printed-circuit-board
PEN	Polyethylene Naphthalate

PET	Polyethylene Terephthalate
PI	Polyimide film
PMMA	Polymethyl Methacrylate
PSD	Power spectral density
RF	Radio frequency
RSU	Remote sense and switch unit
SIS	Semiconductor-insulator-superconductor
SSB	Single side-band
THz	Terahertz
TSP	Temperature sensitive parameter
VDI	Virginia Diodes Inc.
VNA	Vector network analyzer
WGFMU	Waveform generator/fast measurement unit

List of Symbols

A	Amplitude of 1/f noise
A^{**}	Modified Richardson constant
B_i	Constant corresponding to the plateau of a Lorentzian component
C_j	Diode junction capacitance
C_{j0}	Zero-bias capacitance
C_θ	Thermal capacitance
c	Speed of light
D	Electric flux density
d	Thickness of the material sample
E	Electric field
E_{00}	Constant with constant doping density
$e^{\gamma d}$	Phase factor
f	Frequency
f_c	Cutoff frequency
I	Diode current
I_{sat}	Reverse saturation current
k_0	Wave number in free space
k_B	Boltzmann's constant
N	Number of measurement/frequency points
N_{I-tot}	Total noise power spectral density
n	Refractive index
P_T	Dissipated power
q	Electron charge
R_s	Series resistance
R_θ	Thermal resistance
r_a	Diode anode radius
S	Diode junction area

T_0	Ambient temperature
T_j	Diode junction temperature
V	Bias voltage
α	Attenuation factor
β	Propagation factor
ε	Absolute permittivity
ε_0	Vacuum permittivity
ε_r	Relative permittivity
ε'	Real part of the relative permittivity
ε''	Imaginary part of the relative permittivity
η	Ideality factor
ρ_θ	Thermal resistivity
τ	Thermal time-constant
Φ_B	Schottky barrier voltage
ϕ_0	Argument at the first measurement point
ω	Angular frequency
ω_c	Angular cut-off frequency

1. Introduction

The terahertz waves, also known as terahertz radiation or T-waves or THz, consist of electromagnetic waves within frequencies from 0.3–3 THz which corresponds to the wavelengths from 1 mm to $100\,\mu\mathrm{m}$ [1]. Since the THz waves constitute of wavelengths of 1 mm and shorter, it is also termed as submillimeter waves [2]. Besides, the millimeter wave region covers the frequency range from 30–300 GHz with wavelengths from 10 mm to 1 mm. The terahertz and millimeter wave regions lie between the microwave and infrared wave frequencies of the electromagnetic spectrum. Electronic devices like amplifiers and oscillators are used in the microwave band whereas lasers, LED and optical detectors are common for frequencies above 10 THz [3]. But in between, that is in the THz band, none of these technologies are well fitted. Hence, there appears to be a technological gap, the so-called THz gap, in terms of output power and signal detection.

Terahertz and millimeter waves provide several advantages over long electromagnetic waves. At higher frequencies, dimensions are in the range of a wavelength enabling miniaturization of key components and circuit design. Further, the available bandwidth is considerably large compared to that of the microwave frequencies facilitating higher data rate communications. Moreover, strong resonances of some gaseous elements, such as oxygen, ozone and water vapor are observed in the millimeter wave and THz range enabling atmospheric studies using millimeter wave and THz technologies. In imaging applications, a high spatial resolution can be obtained at terahertz and millimeter wave frequencies providing high definition images. Despite the advantages, this frequency range has the drawback of higher atmospheric losses compared to lower frequencies which makes it unsuitable for long range radio communications. Furthermore, at higher frequencies, device fabrication, integration and cost reduction

remain as major challenges.

THz and mm-wave region have been the least explored frequency bands in the electromagnetic spectrum in the past decades. However, the THz and mm-wave technologies are gaining higher interest in the present context due to their wide application areas from radio astronomy [4], earth observation [5], high capacity communication systems [6], and radar [7] to imaging [8, 9], material characterisation [10], biological studies, and medicine [11].

1.1 Motivation, scope and contents of the thesis

The most applicable field of the THz technology these days is in radio astronomy and earth science. High resolution heterodyne receivers are used to study the different astronomical objects and phenomena in space as well as in the earth's atmosphere, for example star formation regions, molecular clouds, planetary atmosphere, comets and the earth's stratosphere [4]. Cryogenic devices, such as superconductor-insulator-superconductor (SIS) and hot electron bolometer (HEB) mixers, are available for THz heterodyne detection. Similarly for THz generation, vacuum tube devices like gyrotons, klystrons and backward wave oscillators (BWO) are in use [3]. These THz detectors, with their cryostats, as well as the generators are large in size and expensive with limited operational life. However, for the space exploration missions, it is desired that the instruments are small, light, compact, durable, and preferably inexpensive. In order to fulfill these requirements, the solid state electronic devices are preferred for THz signal generation and detection.

The Schottky diode is the key component in almost all non-cryogenic mixer and multiplier applications at THz frequencies [12]. In THz receivers, both the mixer and the local oscillator chain multipliers are typically built using Schottky diodes. Hence, efficient characterisation and modelling techniques have a key role in the development of Schottky diode-based devices with a state-of-the-art performance.

Traditionally, performance and quality of the Schottky diodes are accessed with current-voltage (I-V), capacitance-voltage (C-V) and S-parameter measurements. However, these measurements are insufficient to fully charaterise the behavior of the diode under operating conditions. For example, miniaturization of the diode size for the higher frequency applications implies reduced thermal capability and elevates tem-

perature induced effects. The reduced thermal capability and self-heating of the diode have imposed two challenges. First, the characterisation of the diodes using only traditional techniques, such as I-V and C-V measurements, do not provide reliable results on the effect of some diode parameters, e.g., the series resistance is masked by the change of other parameters as a function of the temperature. Second, in many cases thermal constraints have become the limiting factor rather than the obtainable electrical performance. This is especially true when high power varactor diodes are integrated on membrane substrates. To overcome these limitations, a new thermal characterisation method has been developed in this thesis work to extract the diode parameters, such as the peak junction temperature and associated thermal time-constants, under a known input power level. This method is especially suitable for small-size diodes with fast thermal time constants. Measurement based thermal characterisation of the THz diodes is still an interesting topic of study as only very limited work on the thermal analysis of planar Schottky diodes has been carried out so far.

In this thesis, charge trapping effect and low-frequency noise are also studied. This is considered as a complex subject but is of high interest regarding the THz Schottky diode modeling and reliability analysis. Indications of charge trapping in THz Schottky diodes is experimentally investigated with various measurement techniques including current-voltage, capacitance and low-frequency noise measurements.

In addition, performance evaluation of the low-barrier Schottky diodes in terms of conversion loss and effective noise temperature has been made. As the measurement platform, a fundamental mixer test-jig is used with low-loss E-H impedance tuners for RF and LO signal matching. The main objective of this part of the thesis is to evaluate the applicability of the Schottky diode with a low-barrier height in millimeter wave frequency mixing applications.

Furthermore, this thesis includes material characterisation studies at millimeter wave frequencies. Characterisation is based on the transmission line method where the material sample is placed inside a short section of an enclosed transmission line placed between two ports of a vector network analyzer. The reflection and transmission S-parameters measurements are performed in the frequency range from 75 to 325 GHz, and an evaluation of the permittivity and loss tangent is made from direct comparison of measurement results with simulation as well as calculated

values from analytical equations.

1.2 Scientific contributions of the thesis

The scientific contribution of this thesis work has been listed in the following points:

- Development of new verification routine for validating extremely fast pulsed I-V and transient current measurement setups for thermal characterisation of THz Schottky diodes [I].
- Development of a novel method for thermal characterisation of THz Schottky diodes, based on the transient current behavior enabling the extraction of thermal resistances, thermal time-constants, and peak junction temperatures of THz Schottky diodes. The new method can be used to measure small diode devices with thermal time constants down to about 300 ns [II]. The application of the developed method is demonstrated for thermal characterisation of Schottky based prototype mixer and multiplier blocks for MetOp-SG satellite instruments [III].
- Experimental study on charge trapping and low-frequency noise in THz Schottky diodes with various measurement techniques [IV].
- Evaluation of the performance, in terms of conversion loss and noise temperature, of the low-barrier Schottky diodes for millimeter wave mixing applications [V].
- A proposed fast and easy-to-use method for permittivity and loss tangent extraction of a material at millimeter wave frequencies (75 to 325 GHz) [VI]. As an application, the proposed method is used for evaluating suitable polymer materials for printing millimeter wave components [VII].

2. Schottky diode characterisation

Any non-linear electronic device can be used for the purpose of frequency mixing or multiplication. However, at millimeter and THz frequencies, only few devices can provide an acceptable conversion efficiency and low noise performance. Basically, GaAs Schottky barrier diodes are preferred and commonly used in the heterodyne receiver as a mixing element. The reason behind this preference of the Schottky diode over other semiconductor devices is that it does not have any minority carrier storage thus enabling a high speed performance. Further, features such as high mobility, large bandgap and easy processing technology make GaAs the best known choice for a THz receiver element [3, 13]. In recent years, a significant effort has been made on the development of tunable solid state terahertz sources with GaAs Schottky barrier diode based frequency multipliers [12]. The basic principle is to use the nonlinearity, reactive and resistive, of the diode for generating output power at harmonics of the input signal with a good efficiency. Besides, nowadays Schottky diodes are also been used in direct detection [14].

In this chapter, various characterisation techniques applied to the THz Schottky diode are discussed. A novel thermal characterisation method suitable for small Schottky diodes is presented along with its application. Charge trapping and low-frequency noise studies are discussed, and finally, characterisation of low-barrier Schottky diodes for mixer applications at millimeter wave frequencies is presented.

2.1 Schottky diode

In contrast to the p-n semiconductor junction diode, the Schottky diode consists of a metal-semiconductor junction, where a gold or platinum metal contact is established with a semiconductor material, such as silicon or

gallium arsenide (GaAs). N-type semiconductors provide small series resistance and higher cutoff frequency due to its larger carrier mobility and hence are preferred over the p-type semiconductors. The Schottky diode is a majority carrier device, and therefore, does not have the recombination time limitation. These diodes are much faster than the pn-junction diodes, in which the speed is limited by minority carriers [15, 16]. The Schottky diodes can be classified into two categories; resistive (varistor) and capacitive (varactor) diodes. The varactor diodes are used for frequency multiplication purpose whereas the varistor diodes serve as mixers, detectors and multipliers. Compared to varistors, varactors have some advantages, such as high conversion efficiency, high power output, and high breakdown threshold.

GaAs based whisker-contact Schottky diodes were in common use over many years in the millimeter wave frequency range [17–19]. Advantages like a simple structure, small area device fabrication and reduced junction capacitance made these diodes preferable also for the THz receivers. However, due to issues, such as the complexity in assembly with integrated circuits and the reliability, development toward planar structure diode technology has already long been in the focus [20–24]. The planar structure diodes enabled the ability for easy assembling and manufacturing of compact and inexpensive sources and receivers. However, due to the planar structure, an increase in the parasitic shunt capacitance limits the performance of the diodes at higher frequencies. Basically, three design parameters of the GaAs Schottky diode: anode diameter epi-layer doping and epi-layer thickness, can be optimized for its operation in THz frequencies [13]. However, the topic of parameter optimization is not within the scope of this thesis work.

2.1.1 Current-voltage (I-V) and capacitance-voltage (C-V) characteristics

Figure 2.1, according to [25], presents the energy band diagram of the Schottky-junction under four conditions. First, when the metal and semiconductor are not in contact, Figure 2.1.a, the Fermi level in semiconductor is higher than that in metal. The work function, $q\Phi_M$ in metal and $q\Phi_S$ in semiconductor, is defined as the energy difference between the Fermi level and the vacuum energy level. When the metal is in contact with the semiconductor, Figure 2.1.b, electrons flow from semiconductor to metal resulting in positively charged depletion region on the semicon-

ductor side. The flow of electrons continue until the difference between the initial Fermi energy levels is compensated by the developed potential. Due to the accumulation of electrons on metal surface, a potential barrier is formed, known as the built-in voltage. Similarly, electrons on the metal side also experience a potential barrier known as the Schottky barrier. The Schottky junction can be either reverse biased or forward biased. In Figure 2.1.c, reverse bias is applied to the junction meaning the positive voltage is applied to the semiconductor side and the negative voltage to the metal side.

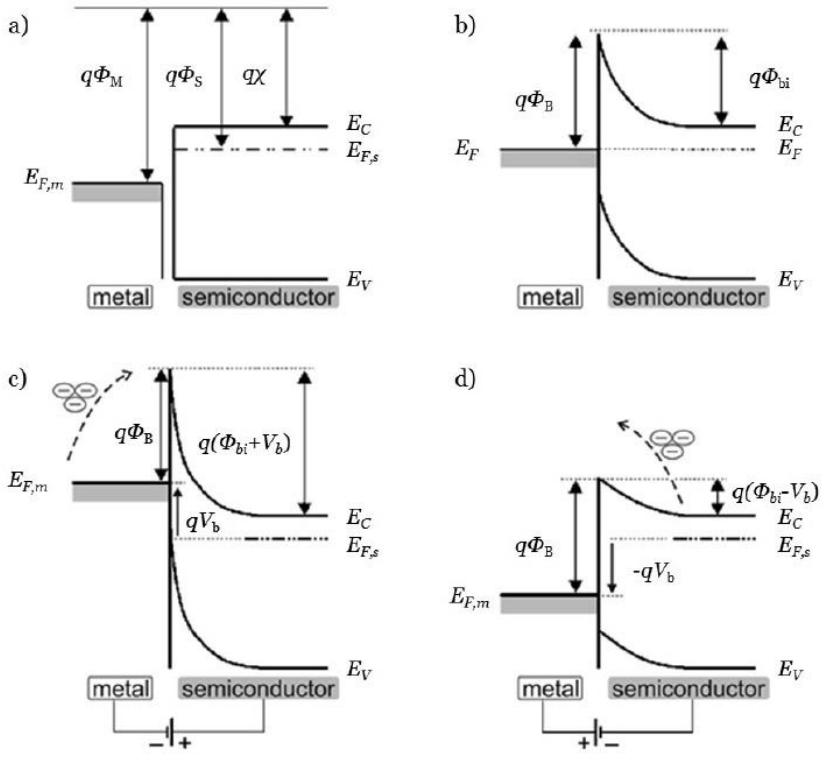

Figure 2.1. Energy band diagram of the Schottky-junction for a) metal and semiconductor not in contact, b) two materials in contact forming a Schottky-junction, c) reverse biased Schottky-junction and, d) forward biased Schottky-junction [25].

In case of forward a bias, Figure 2.1.d, positive voltage connected to the metal side and negative to the semiconductor, the potential barrier is lowered enabling an easy pass for electrons over the barrier. Consequently, the current through the junction increases exponentially with an increase in bias voltage following the thermionic-field emission model as [26–29]

$$I = I_{sat}\left[exp\left(\frac{q(V - IR_s)}{\eta k_B T_j}\right) - 1\right], \tag{2.1}$$

where q is the electron charge, V is the applied bias voltage, k_B is Boltzmann's constant, T_j is the junction temperature, R_s is the series resistance, I_{sat} and η are the reverse saturation current and the ideality factor, respectively, which can be written as [28, 29]

$$I_{sat} = SA^{**}T_j^2 exp\left(-\frac{q\Phi_B}{k_B T_j}\right), \tag{2.2}$$

$$\eta = \frac{q}{kT_j} E_{00} coth\left[\frac{qE_{00}}{kT_j}\right], \tag{2.3}$$

where S is the junction area, A^{**} is the modified Richardson constant (8.2 $\mathrm{Acm^{-2}K^{-2}}$ for GaAs), and Φ_B is the Schottky barrier voltage and E_{00} is a constant with a constant doping density.

Capacitance of a Schottky diode junction is determined by the charge accumulation on both sides of the depletion region and the capacitor size is dependent on the size of the junction, doping density and the applied bias voltage. Mathematically, the junction capacitance of the Schottky diode can be written as

$$C_j = \frac{C_{j0}}{[1 - V/\Phi_b]^{1/2}}, \tag{2.4}$$

where C_{j0} is the zero-bias capacitance.

2.1.2 Frequency conversion in Schottky diode

The nonlinear I-V and C-V characteristics of a Schottky diode can be used for frequency conversion of the signals enabling the possibility to translate the functionality of lower frequency electronics into the higher frequency bands and vice versa. For example, the Schottky diode mixers can down-convert a high-frequency signal to lower frequencies for easy amplification and analysis or up-convert a low-frequency signal to a higher frequency. Further, frequency multipliers can produce harmonics of the signal frequency. If we consider only the room temperature device, GaAs Schottky barrier diodes are known to be the most suitable solid-state device for frequency conversion applications at millimeter wave and THz frequencies.

2.2 Effect of temperature on diode characteristics

The effect of the external environment temperature variation can be observed in the I-V characteristics of the Schottky diode as a shift in the knee (or turn on) voltage. As the temperature rises, the knee moves towards the lower voltage and vice versa, which means that at a constant voltage, the current is larger at a higher temperature. This effect can be observed in Figure 2.2 where the I-V curves of a test diode are plotted for different temperatures.

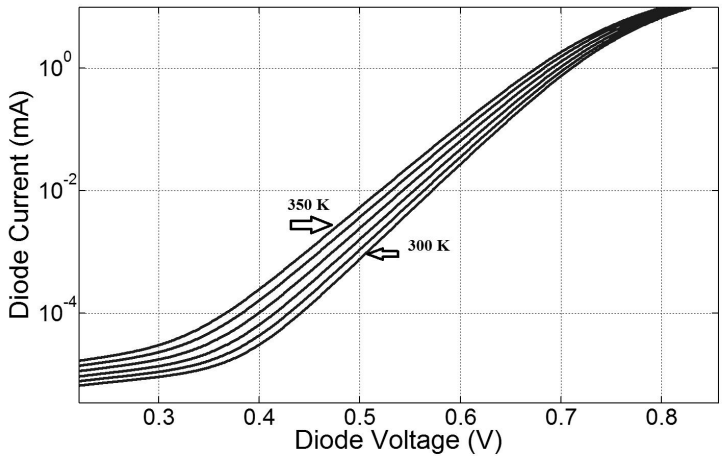

Figure 2.2. Temperature dependent I-V curves for a test diode. Temperature range from 300 K to 350 K. Y-axis in logarithmic scale.

Furthermore, the Schottky diodes experience a self-heating effect caused by the bias current. Hence, the temperature dependence of the saturation current (2.2) and the ideality factor (2.3) plays an important role in characterisation of the thermal and electrical properties of the diode under the operating condition. The temperature of the junction can be estimated using the relation [28, 29]

$$T_j = T_0 + P_T R_\theta, \tag{2.5}$$

where T_0 is the ambient temperature, P_T is the dissipated power in the junction, and R_θ is the thermal resistance of the diode. If we assume that all the power is dissipated in the diode junction, then

$$P_T = V_b I. \tag{2.6}$$

For a circular anode, the thermal resistance can be estimated as

$$R_\theta = \frac{\rho_\theta}{4r_a}, \tag{2.7}$$

where ρ_θ is the thermal resistivity (22×10^{-3} Km/W for GaAs at 300 K) and r_a is the anode radius. In case of a Schottky diode, the geometrical structure and the materials in the vicinity of the anode determine the thermal resistance.

2.3 Thermal charactersation of THz Schottky diodes

Thermal characterisation of a semiconductor device refers to the measurement of the temperature response to the internal self-heating [30]. The semiconductor diode junction heats up as current flows during its operation. The generated heat is large and is concentrated in a small junction region. This heat diffuses out to the package (chip-solder-case) and then eventually to the local ambient according to the laws of thermodynamics and heat transfer. With an increase in the frequency of operation, the size of the semiconductor diode has to be reduced in order to avoid the parasitic effects. However, with the reduced size, the thermal capability, meaning the ability to remove the heat away from the junction, is degraded. The quality and reliability of a semiconductor device depend strongly on its operating temperature [31], because excessive temperature usually implies reduced performance and accelerated aging effects. Hence, thermal characterisation is required for accurate estimation of the junction temperature as a function of time and associated thermal time-constants (chip-solder-case) for thermal modeling of the device self-heating.

2.3.1 Thermal characterisation methods

The literature on various thermal characterisation methods for semiconductor devices is vast [32–38] and the suitability of a particular method is usually determined by the device-under-test (DUT) and the measurement situation. An extensive review on various thermal characterisation techniques for semiconductor devices is given in [31]. In case of small Schottky diode devices, the relevant thermal characterisation methods are thermal modeling methods, imaging methods, and electrical test methods.

Thermal characterisation of Schottky diodes can be performed with the 3-D modeling tools [32–34] which enable the understanding of heat flow

paths inside the device and a comparison with measurement results. Despite the advantages, such as flexibility, fast testing, and no need for the device fabrication, these methods however cannot account for the unexpected fabrication errors and the practical measurement conditions. Imaging methods [35, 36] on the other hand provide a non-destructive approach for determining the temperature and the thermal resistance of the device. However, these methods cannot provide speed, resolution, or penetration of the anode metallization. The electrical test method [30, 37] is a commonly applied method for the thermal characterisation of diodes. However, this method has some limitations when applied in case of small anode area diodes with the fastest thermal time-constants.

In this thesis work, a new thermal characterisation method has been developed for small THz Schottky diodes with fast thermal time-constants [II] which allows the extraction of all the thermal resistances and thermal time-constants associated with the DUT. The fundamental idea is to use the forward diode current as the temperature sensitive parameter (TSP) for the temperature calibration and to measure the transient current resulting from a change in power dissipation. A calibration curve is created by measuring DC I-V characteristics at different controlled temperatures, it is then used to map the measured transient current values to the corresponding temperatures. Finally, the extraction of the thermal parameters is performed by fitting an equation based on the exponential cooling (or heating) law (2.8) to the measured results.

According to (2.5), the steady state junction temperature can be calculated with a constant power level. However, in real-world case, heating or cooling does not take place instantly. To determine how fast a device heats or cools down, it is important to consider the exponential nature of the heat flow and thermal time-constants related to the different parts of the device. For example, when the heating current is turned off, the Schottky diode junction temperature as a function of time can be expressed as

$$T(t) = T_0 + T_1 \times \left(exp\left(\frac{-t}{\tau_1}\right)\right) + ... + T_n \times \left(exp\left(\frac{-t}{\tau_n}\right)\right), \tag{2.8}$$

where

$$\tau_n = R_{\theta,n} C_{\theta,n}. \tag{2.9}$$

Here, $T_n (n > 0)$ is the level of temperature rise related to a thermal resistance of a certain part of the device and τ_n is the corresponding thermal

time-constant. $R_{\theta,n}$ is the thermal resistance associated with this part of the device, and $C_{\theta,n}$ is the corresponding thermal capacitance. The peak temperature of the device can be written as the sum of the temperature levels and the ambient temperature at zero time instant as

$$T(t=0) = T_0 + T_1 + ... + T_n. \tag{2.10}$$

2.3.2 Measurement setup and verification

Measurement setup

In this work, a semiconductor parameter analyzer is used for both temperature dependent DC I-V and transient current measurements. The main advantages offered by the semiconductor parameter analyzer are first, the synchronized source and measurement capability, and second, the simple cabling between the DUT and the system in order to reduce the measurement errors.

Figure 2.3 shows a simple schematic diagram of the setup for I-V and transient current measurements. The semiconductor parameter analyzer, Agilent B1500A (Agilent B1530A Waveform Generator/Fast Measurement Unit), with two source–measurement channels serves as the main instrument in the system. Each of the two channel consists of a remote-sense and switch unit (RSU), where the current–voltage measurement takes place. The input voltage is applied from one channel of the analyzer and the current measurement is performed in the RSU of the other channel. For fast and accurate measurements and a simple cabling setup, the RSU is placed near the DUT.

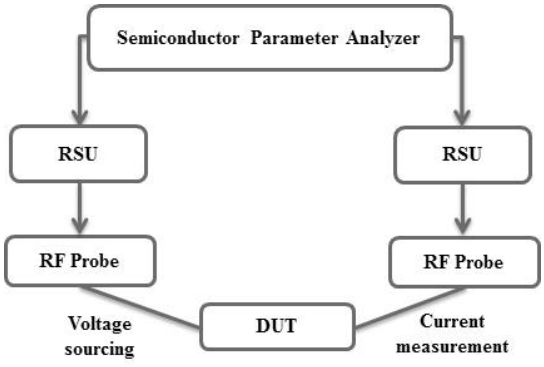

Figure 2.3. Schematic diagram of the measurement system [II].

Figure 2.4 presents the photograph of the measurement setup on the

probe station for thermal characterisation. Single-anode varactor Schottky diodes from Chalmers University of Technology, Göteborg, Sweden, with different anode sizes ($5\,\mu m^2$, $9\,\mu m^2$, and $12\,\mu m^2$), are measured. Each diode is mounted on an on-wafer co-planar waveguide test carrier, which can be contacted with a ground-signal-ground (GSG) RF probes as shown in the figure. The diodes test carriers are placed on the temperature-controlled chuck of the Cascade Microtech probe station. Each measurement is performed in the temperature range of 283 to 333 K with steps of 10 K. For temperature control, Temptronic Corporation Thermal Platform is used and the thermal chuck is shielded in order to obtain temperature uniformity over the chuck.

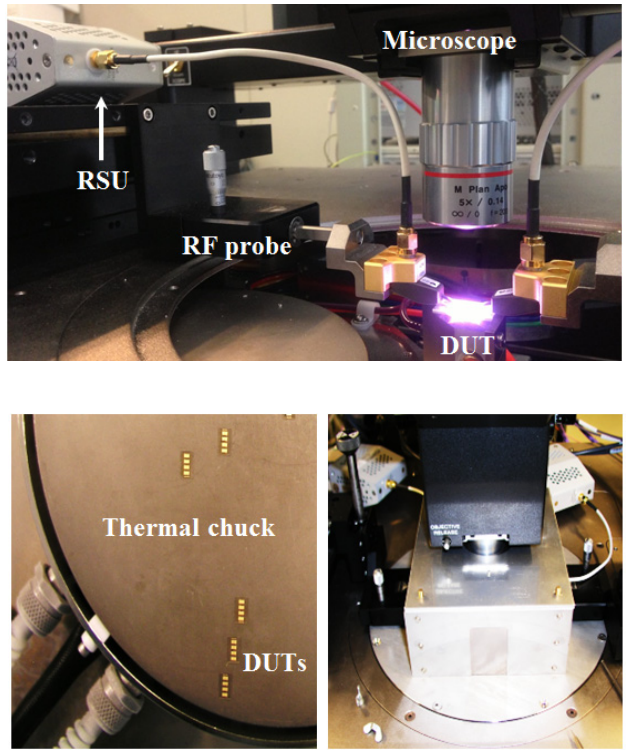

Figure 2.4. Photograph of the measurement setup on probe station. DUTs are placed on the temperature-controlled chuck and the shielding is applied around it [II].

Verification

Reliability of the developed thermal characterisation method depends on the accuracy of the measurement system. Measurement of the DUT outside the specified range reduces the accuracy in an unknown way. Hence, a verification routine is essential in order to make sure that the measurement parameters, such as the DUT resistance, heating/measurement

current levels, and current setling time are within the verified range during the measurement of the DUT. To fulfill this requirement, a verification routine for transient current measurement setup has been developed in [I]. It is applied beforehand the actual transient current measurements for accurate thermal characterisation of the DUT.

2.3.3 Characterisation procedure and results

The developed new thermal characterisation method involves three main steps. The first step is the generation of the current-temperature calibration curve from temperature dependent I-V measurements for each DUT. I-V measurements are made at different temperatures and a heating current and measurement current levels are selected. The heating current level is in the range of few mA and the measurement current is selected at sufficiently lower value without creating significant self-heating of the diode. Current-temperature relationship is then established by recording the current levels at different temperatures for a selected voltage value (corresponding to the measurement current level). Figure 2.5 shows the calibration curves obtained for each diode type from temperature dependent–measurements.

The second step involves the measurement of the transient current resulting from the change in power dissipation. This means that the diode is heated until it reaches the steady state at thermal equilibrium by applying the heating voltage. After the heating period, the voltage level is changed to the measurement voltage and the corresponding transient current response is measured. Figure 2.6 presents the transient current measurement results for diodes with three different anode sizes.

The third and final step is the extraction of the thermal parameters. A cooling curve (response) is created by mapping the measured transient current values to the corresponding temperature values of the diode with the help of the calibration curve. The cooling curve contains all of the information necessary for thermal parameter extraction. The thermal time-constants and the temperatures corresponding to the intermediate equilibrium stages are extracted using the least squares error curve fitting technique with (2.8). Finally, extraction of the peak junction temperature is performed using extrapolation of the cooling curve. Figure 2.7 represents the heat flow path from the hot junction to the local ambient through intermediate thermal stages of the diode.

The extracted thermal parameters of the diodes are presented in Table

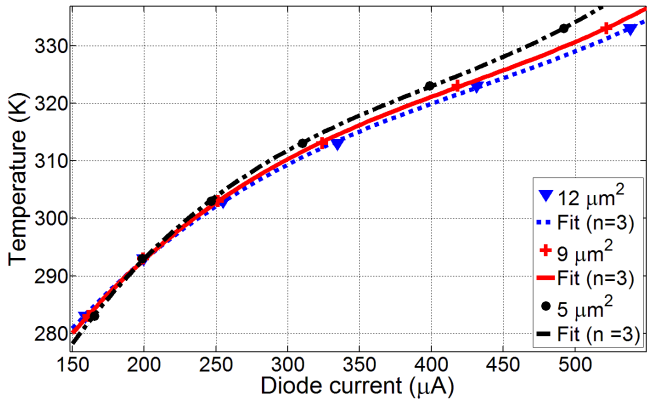

Figure 2.5. Calibration curves for varactor diodes with different anode sizes [II].

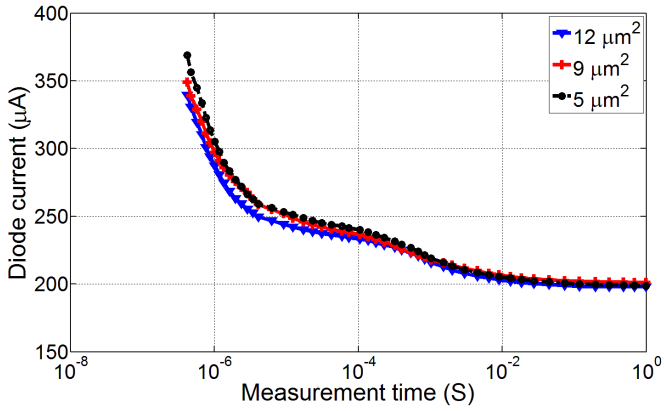

Figure 2.6. Transient current measurement results for varactor diodes with different anode sizes [II].

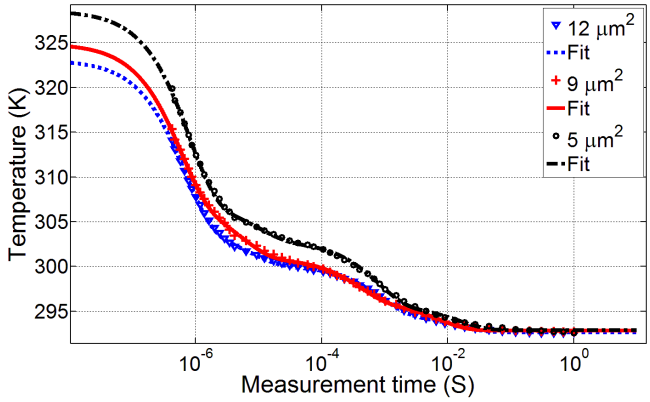

Figure 2.7. Thermal response plots of different anode size diodes. The smallest diode heats up the most as expected [II].

I. The ambient temperature in this case is 293 K. From the data, it can be observed that the extracted peak junction temperature is larger in a smaller area anode diode than in a larger area diode, as expected. Table II presents the extracted temperature levels and thermal resistance corresponding to different parts of the diode. A comparison between the thermal parameter extraction results using the new method, two 3-D simulation tools (ANSYS Mechanical and COMSOL Multiphysics), and an in-house thermal characterisation method [38] are presented in Table III. In case of a Schottky diode with an anode area of $9\,\mu\mathrm{m}^2$, the thermal characterisation result for the total thermal resistance is within 10 $\%$ of the average value of 4020 K/W when using all four approaches.

2.3.4 Measurement uncertainty

The uncertainties in thermal characterisation measurements are related to the electrical transients of the measurement system, the measured transient current, and the temperature accuracy of the thermal platform. The largest contributor to the uncertainty are the very first current points after the change from heating to the measurement voltage level. This is caused by the electrical transients and need to be suppressed before actual measurements of the DUT. From the verification routine [I], it is observed that the measured transient current points 250–300 ns after the change in voltage level can be used for thermal parameter extraction purpose. To ensure that the fastest time-constant is larger than 250 ns in the DUTs, ANSYS and COMSOL 3-D thermal simulations are performed.

An error analysis is performed by changing the starting time points in the measured transient current data used for the extraction. With the different starting points, the error in the extracted peak junction temperature is $\pm$ 3.0 K and that in the thermal resistance is $\pm$ 450 K/W.

The transient current is measured using the Agilent semiconductor parameter analyzer with the uncertainty of 0.1 $\%$ of the reading. The noise floor of the system is 0.2 $\%$ of the measurement range. The Temptronic Corporation Thermal Platform has a temperature accuracy of 0.5 K with the temperature stability of 0.1 K. The chuck temperature uniformity is 0.5 K. By using the Monte Carlo analysis, an estimate of the total error in the peak temperature and thermal resistance extraction is calculated to be approximately $\pm$ 4.2 K and $\pm$ 570 K/W, respectively.

TABLE I
EXTRACTED THERMAL PARAMETERS OF THE DIODES [II]

Anode area (μm^2)	Peak temperature (K)	Ambient temperature, T_0 (K)	Time constants (s)				Power, P_T (mW)	Total thermal resistance, R_θ (K/W)
			τ_1	τ_2	τ_3	τ_4		
5	328.3 ± 4.2	292.8	$7.8 \cdot 10^{-7}$	$1.1 \cdot 10^{-6}$	$8.1 \cdot 10^{-4}$	0.016	7.82	4530 ± 570
9	324.4 ± 4.2	292.4	$5.7 \cdot 10^{-7}$	$5.7 \cdot 10^{-6}$	$4.1 \cdot 10^{-4}$	0.017	7.35	4350 ± 570
12	322.7 ± 4.2	292.3	$6.7 \cdot 10^{-7}$	$7.8 \cdot 10^{-6}$	$8.9 \cdot 10^{-4}$	0.015	7.20	4200 ± 570

TABLE II
EXTRACTED TEMPERATURE LEVELS AND THERMAL RESISTANCES RELATED TO DIFFERENT REGIONS OF THE DIODE [II]

Anode area (μm^2)	Temperature rise, T_n (K)				Thermal resistance, $R_{\theta,n}$ (K/W)			
	T_1	T_2	T_3	T_4	$R_{\theta,1}$	$R_{\theta,2}$	$R_{\theta,3}$	$R_{\theta,4}$
5	21.6	4.2	7.2	2.8	2740	520	900	340
9	19.3	5.3	5.1	2.3	2620	720	690	310
12	18.5	4.1	5.4	2.1	2560	560	750	290

TABLE III
COMPARISON OF THE EXTRACTED THERMAL PARAMETERS [II]

Method	Change in temperature, ΔT_J (K)	Total thermal resistance, R_θ (K/W)
New method	32.0	4350
ANSYS simulation	28.7	3900
COMSOL simulation	26.8	3640
In-house method	30.8	4190

2.3.5 Advantages and applications of the developed thermal characterisation method

Advantages

The main advantages (or differences) of the new thermal characterisation method compared to the standard electrical test method can be summarized in three points. First, this method avoids pulse-heating problem that appears in the standard electrical test method where current pulses of different widths are applied for heating up the diode. In that case, the temperature of the diode rises with fast pulse excitation thus changing the power dissipation, which implies a reduced accuracy in determination of the junction temperature. In the new developed method, the diode is heated up to the steady state thermal equilibrium and hence avoids the aforementioned problem.

Second, this method uses the diode current as the temperature sensitive parameter instead of the diode voltage. Theoretically this is insignificant. However, when we consider building a practical measurement setup, obtaining a suitable heating current levels with sub-microsecond pulses is not possible with the current state-of-the-art synchronized source-and-measure equipment. However, the equipment for voltage pulsing with sufficient voltage levels and sub-microsecond (even 300 ns) pulses is commercially available [39, 40]. The only drawback of this selection is the generation of a non-linear calibration curve which requires extra temperature controlled I-V measurements.

Third, with the new method, it is possible to extract all the thermal parameters from a single transient measurement. A cooling curve provides all the information required to fully characterise the diode's thermal performance. One more advantage of this method is the ability to source and measure at different terminals enabling the isolation of the terminals with the DUT.

Application

The new thermal characterisation method can be used in the process development, electro-thermal modeling, and in reliability analysis of Schottky devices. One of the applications where the thermal characterisation of Schottky devices plays an important role is the space missions where the devices have to operate over a long period of time without the possibility of repair or replacement. Thermal impedance measurements are

extremely important to determine the life time testing conditions of these devices, and to evaluate their reliability. The Schottky diode technology is used for frequency conversion and generation in three of the mm-wave and THz instruments on-board the European Space Agency's MetOp-SG satellites. In this thesis work, the thermal characterisation is performed for Schottky diodes used in these instruments as a part of the reliability assessment process [III]. Different multiplier and mixer prototype modules have been thermally tested in addition to the thermal simulations.

Measurement setup for this task consists of a semiconductor parameter analyser, a heating oven and a temperature sensor as shown in Figure 2.8. Here, only one channel of the semiconductor parameter analyser is used for I-V characteristics and transient current measurements. The added advantage of this setup is the ability to measure RF and thermal properties from only one port (DC bias port) of the prototype blocks. This implies that there is no need of mounting diodes on a separate module blocks for the characterisation purpose.

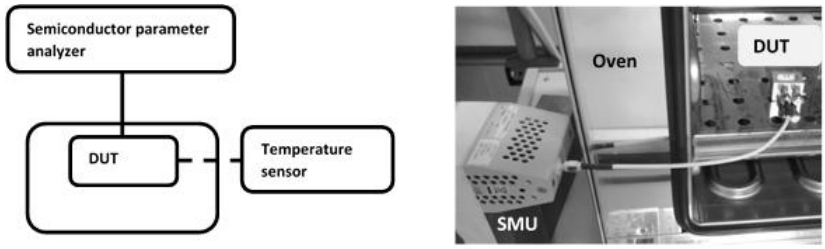

Figure 2.8. Block diagram of the measurement setup and photograph of the prototype block (inside the oven) connected to the remote-sense and switch unit (RSU) of the semiconductor parameter analyzer [III].

In addition to the thermal measurements, also RF measurements are performed for three identical multiplier prototype blocks. The results indicate that the block with a poor thermal performance (large peak junction temperature) has small output power as well as low efficiency. This implies that the developed thermal characterisation method can be used to study the interrelation between the thermal and RF performance of the devices. Further, the method can be applied to check the reproducibility of the assembly of discrete devices.

2.4 Charge trapping and low-frequency noise in THz Schottky diodes

Traps in a semiconductor device are known or implied to be a cause of many unidealities in the device operation. Regarding the characterisation of Schottky diodes, reported problems include at least irregularities in I-V and C-V measurements, possibly sometimes even making the characterisation impossible in practice. As traps include charge capture and release effects, it is obvious that their effects may contribute to some error in the characterisation and extraction of electrical parameters and indirectly also in the derived thermal parameters. Besides, a variation in the characteristics of a device performance is usually specified by the noise. In semiconductor devices, low-frequency (LF) noise relates to the fluctuation in the charge transport which is determined by carrier scattering and trapping effects. Further, the majority of failures in electron devices are known to be caused by defects during the manufacturing process or operation [41]. Low frequency noise measurements can be used as a diagnostic method to identify defects and failures in semiconductor devices as this noise is sensitive to the defects. Hence, accurate measurement of the LF noise can provide valuable information on the device quality and its reliability [42].

Studies regarding charge trapping and subsequently the LF noise is vital for the Schottky diodes especially when used in mixer and diode detector applications. In the mixer with a low intermediate frequency case, the low-frequency noise (due to traps) can be up-converted to higher frequencies limiting the performance of the mixer device. This is actually true also in multiplier chains, where multipliers are used to get signal at a higher frequency [43]. Besides, at large input power levels, the low-frequency noise mechanism is dominant which determines the performance of the Schottky-based diode detectors. Hence, characterisation of the detector requires measurement of the diode noise behavior across the operating range of input power levels [44, 45]. Furthermore, low-frequency noise can also cause phase noise in oscillator circuits and it limits the system sensitivity in small-signal mixer applications at microwave and millimeter wave frequencies [46].

In general, the quality of the interface between semiconductor and metal determines the performance and reliability of a Schottky diode [47–49]. There is plenty of literature available on various methods for character-

isation of trap states in a Schottky diode. Investigation of the traps in Schottky diodes are usually performed by current-voltage (I-V) [50, 51], frequency dependent capacitance, conductance and admittance measurements [52–54]. Besides, deep-level transient spectroscopy (DLTS) methods are well known as a unique and powerful tool for study of electrically active defects in semiconductors [55–60]. However, these methods are not suitable for THz Schottky diodes with a small capacitance (in the fF range). On the other hand, a noise spectroscopy technique has also been used as a tool to study defects in semiconductors [61, 62]. In the case of Schottky diodes, low-frequency noise has been studied widely [63–72] because noise spectroscopy is a more feasible technique for characterising such small area devices compared to the conventional DLTS techniques.

2.4.1 Measurements and results

In this thesis work, experimental investigation has been carried out in order to study the indication of charge trapping in THz Schottky diodes with various measurement techniques including current-voltage, capacitance and low-frequency noise measurements [IV]. Measurements are made in on-wafer environment using a probe station and GaAs diodes from various manufacturers are tested.

From the measurement results it is observed that with the I-V and C-V measurements alone, it is challenging to identify the presence of traps in the DUT. The capacitance measurements provide some indication about the presence of traps. It was evident that the most suitable methods to investigate the trapping effect, in small area Schottky diodes, are capacitance-frequency and the low-frequency noise measurements as both methods reveal the presence of traps (if any) in the DUT and also exhibit strong correlation between the measurement results.

In the low-frequency noise measurements, the measured noise power spectral density (PSD) provides the information about the number of distinct trap levels which is determined by the number of Lorentzian levels it exhibits. For example, Figure 2.9 presents the total measured PSD that can be fitted with the combination of the 1/f noise, two Lorentzian noise components (GR1 and GR2) and shot noise. Each Lorentzian component is associated with a trap level, characterized by a discrete energy level and a time-constant. The corner frequency of the Lorentzian spectrum (f_c) provides the trap time-constant ($f_c = 1/2\pi\tau$). Mathematically, the total noise PSD can be expressed as

$$N_{I-tot} = \frac{A}{f} + \sum_{i=1}^{n} \frac{B_i / f_{ci}}{1 + (f/f_{ci})^2} + \text{Shot noise}, \tag{2.11}$$

where A is the amplitude of 1/f noise and B_i is the constant corresponding to the plateau of a Lorentzian component.

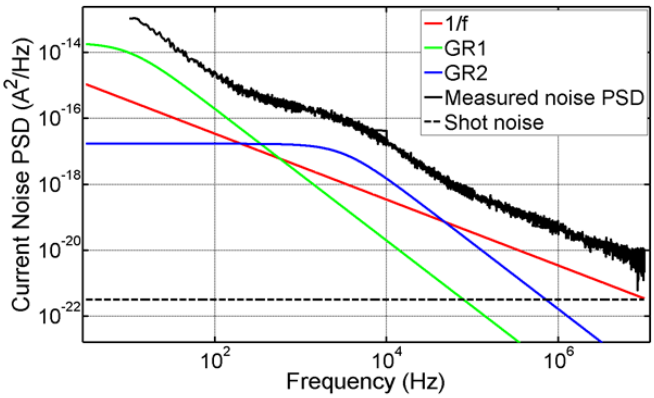

Figure 2.9. Decomposition of the PSD into 1/f and Lorentzian components [IV].

From the least square error curve fitting of the noise PSD, the 1/f noise and generation-recombination noise parameters can be extracted. An illustration plot of a diode sample is shown in Figure 2.10 which presents the fitting of the measured PSD with (2.11) at 1 mA current bias level. The current level of 1 mA is relatively large for the detector diodes. However, in case of multiplier and mixer diodes (measured in this work), this value is realistic if they are pumped with high RF power (few mW). The characteristics frequencies at 10 Hz and 3 kHz are identified corresponding to the time-constants of 15.9 ms and $53\,\mu s$.

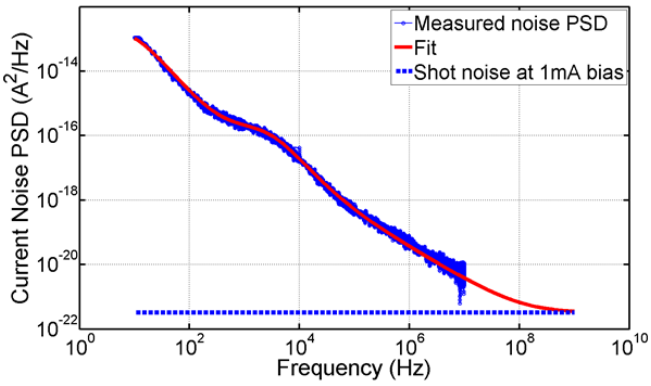

Figure 2.10. Least square curve fitting of the measured PSD [IV].

Several measurements were made in order to insure the repeatability

of the results. The effect of light on the measurement results was found to be negligible. The origin of the trap states in the THz Schottky diodes are not fully understood, howerve, they can be related to the unwanted impurities and defects present in the GaAs layer during fabrication.

2.5 Characterisation of low-barrier Schottky diodes for millimeter wave mixer applications

Considering only the room temperature devices, Schottky diode frequency mixers have been the most suitable selection for heterodyne receivers at millimeter and sub-millimeter waves. However, at higher frequencies, a major limitation of these devices is the difficulty in obtaining sufficient local oscillator (LO) power from solid state sources. One approach to address this problem is to use sub-harmonically pumped anti-parallel GaAs diode pairs where the LO frequency is halved. However, for optimum conversion efficiency and high LO power requirements still exists. For example, a state-of-art sub-harmonic mixer based on GaAs Schottky diode requires 3 mW to 5 mW of LO power. Hence, it is desirable to obtain a mixer that can operate with a lower LO power with an acceptable conversion efficiency and noise temperature. The LO power requirement can be significantly reduced by replacing the GaAs diodes with the low-barrier Schottky diodes where the barrier height can be lowered. For example with InGaAs this can be achieved by increasing the indium mole fraction. Along with the reduction in the LO power requirement, an added advantage of using a low-barrier diode is its high electron mobility, compared to the GaAs diodes, which leads to lower series resistance and, eventually, to better conversion efficiency. Recent studies [73, 74] showed that the mixer based on low-barrier Schottky diodes may require LO power in order of few hundreds of microwatts which is considerably lower than that required by the GaAs based mixers.

In this thesis work, characterisation measurements and simulations have been performed with InGaAs low-barrier Schottky diodes from ACST GmbH, Germany [V]. The diode features the anode diameter of $1.5\,\mu\mathrm{m}$, the differential resistance (known also as the junction resistance at zero bias, R_{diff}) of 3150 Ω, the DC current responsivity of 14.4 A/W and diode the substrate dimensions of $147\times46\,\mu\mathrm{m}^2$, with $4\,\mu\mathrm{m}$ height. Although these diodes have been fully characterised for low power detector applications, their performance as mixers has not been tested yet. Hence, the suitabil-

ity of such diodes for millimeter wave mixing applications is studied in this work by evaluating the key performance parameters, such as the conversion loss and noise temperature. As a measurement platform, a fundamental mixer test-jig [75] is used that consists of low-loss E-H impedance tuners for matching RF and LO signals. Furthermore, 3D diode models are created and simulated in High Frequency Structure Simulator (HFSS) and circuit simulations are performed in Advanced Design System (ADS) to compare with the measurement results.

2.5.1 Measurement setups and results

Conversion loss and noise temperature are the two key parameters evaluated in this work. Figure 2.11 presents the experimental setup for conversion loss measurement where G-band amplifier/multiplier chain (AMC), from Virginia Diodes Inc. (VDI), serves as the LO source at 182 GHz. For a coherent RF source, an Agilent vector network analyzer (VNA) along with the Oleson V05VNA2-T/R extension unit is used that provides the RF signal to the mixer at 183 GHz. The intermediate frequency (IF) output, at 1 GHz, is measured with the power meter/spectrum analyzer.

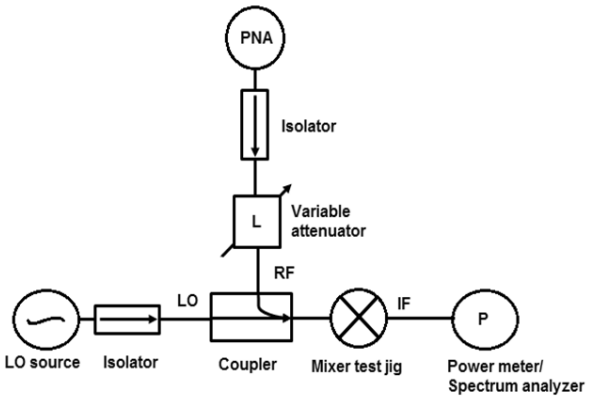

Figure 2.11. Experimental setup for conversion loss measurement with a coherent RF source [IV].

From the measured output power at the IF port, single side band (SSB) and double side band (DSB) conversion losses are calculated as [76]

$$L_{SSB} = \frac{P_{RF}}{P_{IF}}, \tag{2.12}$$

$$L_{DSB} = \frac{L_s L_i}{L_s + L_i}, \tag{2.13}$$

where P_{RF} is the measured RF power at the input of the mixer, P_{IF} is the measured IF power, L_s is the SSB conversion loss at signal frequency (183 GHz) and L_i is the SSB conversion loss at image frequency (181 GHz).

Figures 2.12 and 2.13 present the measured SSB and DSB conversion losses as a function of LO power at both the signal and image frequencies. It is evident from the plots that the IF impedance tuning (with a stub tuner) significantly improves the conversion efficiency of the mixer. At 0.1 mW of LO power, DSB conversion loss of less than 5 dB is obtained which indicates significant reduction in the LO power requirement for mixer operation when using the low-barrier diode under test.

For noise temperature measurements, the setup shown in Figure 2.14 is used where the so called Y-factor method [76, 77] is applied in order to obtain the mixer equivalent noise temperature. The IF chain consists of an IF tuner, an isolator, and a low-noise amplifier. The IF output from the mixer is connected to an isolator with a matched load termination. The RF port of the mixer is used to apply the hot (absorber at 296 K) and the cold (liquid nitrogen at 77.5 K) loads to the mixer and the respective hot and cold noise powers are measured from the IF port. As an LO source, a Gunn+doubler combination is implemented because it contributes less noise compared to the VDI AMC.

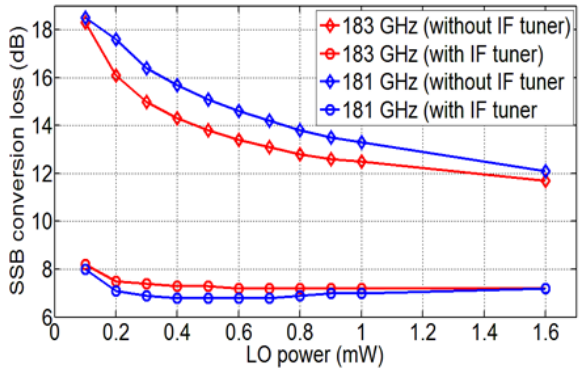

Figure 2.12. SSB conversion loss measurement results [IV].

With the known hot and cold noise power, the Y-factor and consequently the effective noise temperature of the whole setup can be written as

$$Y = \frac{P_H}{P_C} = \frac{T_H + T_e}{T_C + T_e}, \tag{2.14}$$

$$T_e = \frac{T'_H - YT'_C}{Y - 1}, \tag{2.15}$$

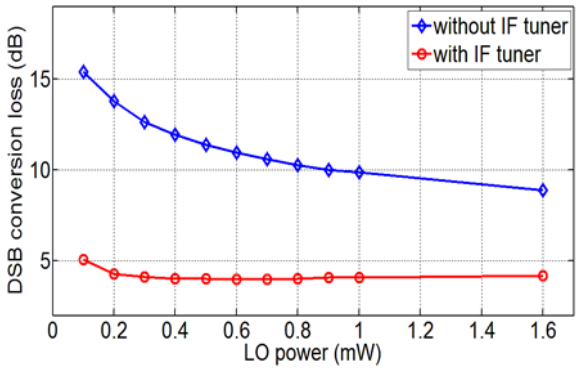

Figure 2.13. DSB conversion loss measurement results [IV].

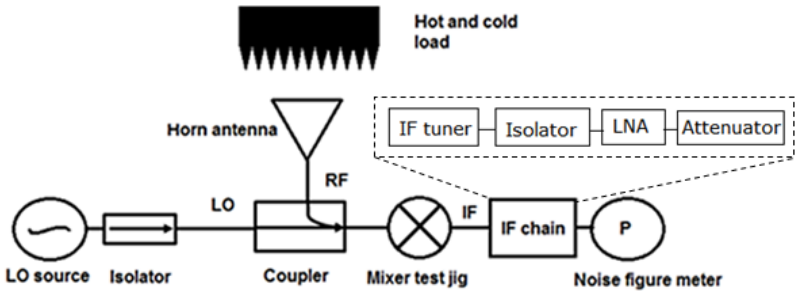

Figure 2.14. Experimental setup for noise temperature measurements. IF chain consisting of an IF tuner, an isolator, a low-noise amplifier and an attenuator.

where P_H and P_C are the noise power with hot and cold load, respectively, and T_H and T_C are the noise temperatures of the hot and cold loads, respectively. $T_H^{'}$ and $T_C^{'}$ are the corrected hot and cold noise temperatures that take into account the attenuation in the RF path including the horn antenna, waveguide section and coupler. These noise temperatures can be calculated as

$$T_{H,C}^{'} = \frac{T_{H,C}}{L_{RF}} + \left(1 - \frac{1}{L_{RF}}\right) T_0, \tag{2.16}$$

where L_{RF} is the total attenuation in the RF path and T_0 is the ambient temperature.

Two measurements approaches have been implemented to evaluate the noise temperature in the work. First, with the direct measurements where the noise temperature is simply calculated by measuring the output noise power with the noise figure meter and applying the Y-factor method. The effect of the IF chain in the measurement setup is calibrated out with the same noise source (diode) as used for calibrating the noise fiugre meter.

The noise source is connected to the input of the IF chain and then the calibration is performed, meaning the noise figure meter is calibrated to the output port of the IF impedance tunner.

Second, with a variable attenuator in the IF chain where the hot and cold noise powers are measured at different adjustments of the variable attenuation of the IF chain (0 to 20 dB). This approach requires two individual measurements, namely that of noise temperature of the IF chain (with the attenuator) and of noise temperature of the whole setup. The linear dependence of the IF chain noise temperature to the noise temperature of the whole setup can be written as

$$T_e = T_M + L_{DSB} T_{IF}, \tag{2.17}$$

where T_M is the mixer noise temperature and T_{IF} is the noise temperature of the IF chain. Solving this equation, the mixer noise temperature and the DSB conversion loss can be calculated.

Figure 2.15 presents the comparison between the noise measurement result obtained from the two approaches. The measured noise temperature from the variable attenuation method appears to be higher than that obtained from the direct noise measurement. This might be attributed to the fact that the accuracy of the attenuation method partly depends on the number of attenuation points considered during the measurement because the larger the number of attenuation points, the better the accuracy of the curve fitting, and consequently an improved accuracy in the noise temperature results. However, the differences in the results obtained from these approaches are not fully understood. It is speculated that the postion of the attenuator after the LNA (see Figure 2.14) might have caused such a large uncertainty in the results since a large attenuation is needed in order to affect the system noise temperature. Hence, further studies are required to determine these effects.

2.5.2 Simulation results

A 3D-diode model is built and added to the mixer test jig 3D-model in HFSS. Then the S-parameter simulations are performed and the results are exported to the ADS circuit simulator. The diode's electrical parameters, such as the series resistance, junction capacitance, saturation current etc., are defined in ADS representing the diode junction and then the evaluation of conversion loss and noise temperature is preformed with

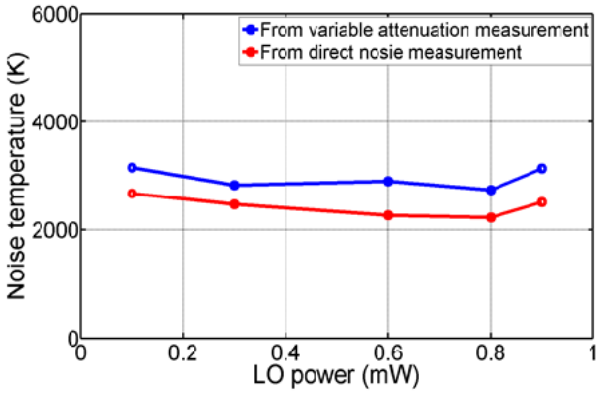

Figure 2.15. Noise temperature for mixer diode obtained from two noise measurement approaches [IV].

harmonic balance analysis. Figure 2.16 shows a snapshot of the 3D-diode model mounted in the test carrier and placed inside the mixer test jig. The ADS circuit simulation schematic is presented in Figure 2.17.

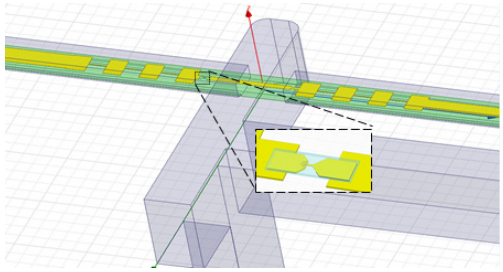

Figure 2.16. HFSS simulation model consisting of EH-tuner, waveguide-to- suspended microstrip transition, DC/IF filter, and the diode model [IV].

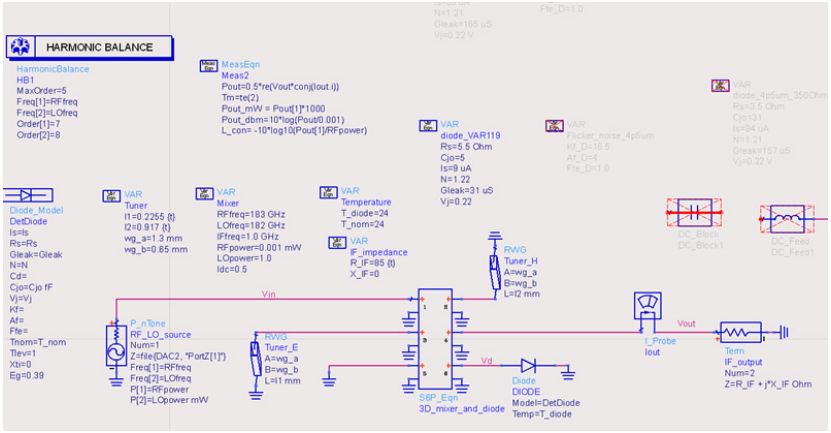

Figure 2.17. Example circuit schematic of the simulation setup in ADS [IV].

Initially, the simulations are performed for three different contributions

of the flicker noise (K_f equals to 16.5, 2, and 0.5). However, comparison of measurement and simulation results indicates that the actual noise model, valid for low-power detector design, is invalid when designing low-power mixers. Hence, new diode models are obtained with different values of differential resistance. From this approach, better results are obtained as shown in Figure 2.18. The new diode model showed improvement in the mixer performance with significant reduction in noise temperature compared to the earlier diode model. At the moment, these diode models are only tested with simulation as the new diodes are being fabricated and measurements are required to verify the simulated mixer performance.

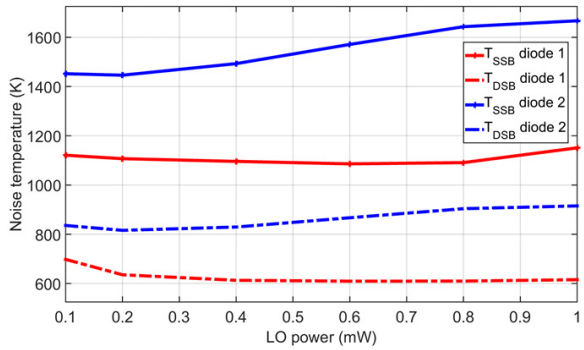

Figure 2.18. Simulated SSB and DSB noise temperature results with new diode models as a function of LO power. Diode 1 with 10 kΩ and diode 2 with 1 kΩ differential resistance.

3. Material characterisation

Accurate knowledge about the electromagnetic properties of the substrate material at the operating frequency is a preliminary requirement from the design point of view. Measurement of the dielectric properties of the material is an important tool to understand the material behavior especially at high frequencies as it can provide the electrical or magnetic characteristics of the materials. This information is a critical parameter required to implement the material in many microwave and mm-wave applications. Besides, various application areas, such as material science, communication, circuit design and biological studies require information on the complex dielectric properties of the materials [78, 79].

3.1 Material measurement at millimeter wave frequencies

In the past years, different dielectric materials have been characterized at lower (microwave) frequencies. However, accurate measurement of such materials at millimeter wavelengths still remains difficult. Recently, application areas of mm-waves, such as high data-rate transmission, automotive radars and sensors [80–83] have gained considerable attention of the researchers for development of the future technologies. At these frequencies, electrical performance of the devices depend strongly on the properties of printed-circuit-board (PCB) or substrate materials. Hence, it is important to fully characterise the material in terms of thickness, dielectric constant, dielectric losses and other relevant electrical parameters to obtain optimum device performance at mm-wave frequencies. For example, future generation cellular networks that use 5G (Fifth Generation) technologies may require compact microstrip antennas where the selection and characterisation of the substrate material is a prerequisite for antenna designers. Furthermore, printing of electronics structures

over a polymer is considered to be a promising method for manufacturing electronic devices at mm-wavelengths due to the reduced costs and better flexibility. In such a case, it is vital, from the design point of view, to carefully obtain the polymer material dielectric properties.

3.1.1 Dielectric material properties

Any material is termed as dielectric if it has the ability to store energy when an external electric field is applied [84]. Electric displacement (or electric flux density) D is defined as,

$$D = \varepsilon E, \tag{3.1}$$

where ε = $\varepsilon_0\varepsilon_r$ is the absolute permittivity, ε_r is the relative permittivity, $\varepsilon_0 = \frac{1}{36\pi} \times 10^{-9}$ F/m is the vacuum permittivity and E is the external electric field. Dielectric constant, also known as relative permittivity, ε_r, is defined as the ratio of absolute permittivity (ε) to the permittivity of the vacuum, ε_0. It is a complex quantity and is represented as [85]

$$\varepsilon_r = \frac{\varepsilon}{\varepsilon_0} = \varepsilon' - j\varepsilon'', \tag{3.2}$$

where ε' is the real part of permittivity that represents the measure of stored energy in a material and the imaginary part, ε'', is the loss factor that provides the measure of how lossy a material is to an applied external electric field.

Loss tangent, also denoted by tanδ, is the ratio of the imaginary part of the permittivity to the real part and can be expressed as

$$\tan\delta = \frac{\varepsilon_r''}{\varepsilon_r'}. \tag{3.3}$$

3.2 Characterisation methods for dielectric materials

Over the past few decades, various methods have been developed for evaluation of the electromagnetic properties of materials. An overview on the available measurement methods for dielectric material characterisation can be found in [86]. Selection of an appropriate method for a particular application is determined by the factors, such as the desired measurement

accuracy, measurement frequency range, convenience, cost, and shape (or form) of a sample material. Commonly used techniques include free-space method [87], coaxial-probe technique [88], cavity resonators [89], dielectric resonator [90], and transmission-line techniques [91–93].

Each method has its advantages and limitations depending on the application area and the material under test (MUT). The resonator techniques are accurate and are useful for measuring low-loss materials but they are narrow banded. The free-space method is considered more convenient for broadband measurement but has lower accuracy and is suitable especially for large material samples. The coaxial-probe method can provide broadband results and is suitable especially for studying liquids and semi-solids. The transmission-line method, on the other hand, is suitable for measuring lossy to low-loss MUTs in a broad frequency range.

3.3 Transmission line method

In this thesis work, a fast and easy-to-use technique based on the transmission line method has been demonstrated to extract the dielectric parameters of the sample MUTs at millimeter wave frequencies [VI]. The full two-port scattering parameters are measured over the frequency range of 75–325 GHz by a vector network analyser. A precisely prepared material specimen is inserted in a section of a waveguide (sample holder) and is placed between the test heads. The reflection and transmission coefficient magnitude and phase are measured and the estimation of the dielectric parameters is made first with the direct comparison to the simulation results and second from applying analytical formulas relating the S-parameters and the material sample permittivity.

3.4 Specimen preparation, measurements and simulations

Accuracy of the S-parameter measurements and, consequently, that of the extracted dielectric parameters depends on the quality of the material specimen. Hence, careful preparation of the test samples is vital. A test material is cut carefully and inserted into a steel holder (thickness of 0.5 mm) which matches the waveguide opening dimension of the measurement frequency band. In this work, material measurements are carried out in four frequency bands (WR10, WR06, WR05, and WR03) covering

the frequency range from 75–325 GHz.

Measurement setup consists of a vector network analyser with a millimeter wave head controller and two external synthesisers, and two waveguide test heads. The waveguide test heads are available for each frequency bands. The measurement configurations as well as the waveguide test heads and the sample holders need to be changed for measurement in different frequency bands. Figure 3.1 presents the photograph of the full two-port S-parameter measurement setup with a material specimen placed between the waveguide test heads. To obtain the loss added by the steel holder, S-parameter measurements are performed for an empty holder (without any material inside) as a reference measurement. Then, the material specimen is measured over the whole frequency band (75–325 GHz). In this work, two types of material samples were tested. First, with a Teflon test sample whose permittivity is well known, and second, with a polymer whose dielectric parameters are unknown.

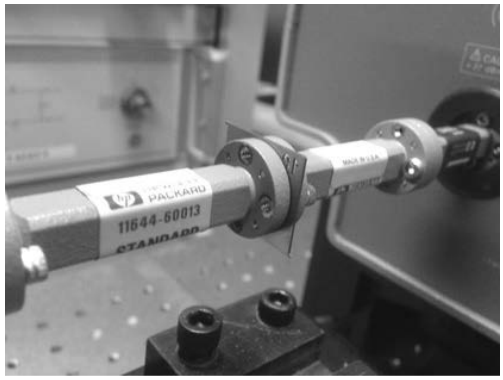

Figure 3.1. Photograph of the S-parameter measurement setup. The material sample is placed between the waveguide test heads [VII].

Material measurement scenarios are simulated in commercial a 3D simulation software (HFSS) in the same frequency range of 75–325 GHz. First, an empty space is simulated as a reference which represents the empty holder case in the measurement. Second, a section of the waveguide representing the material sample is inserted between the waveguide blocks as shown in Figure 3.2. Simulated reflection and transmission coefficients are recorded for various sets of data for different dielectric constant and loss tangents using a parametric sweep. Finally, the simulation data sets are compared to the measured S-parameters to obtain the best least square fit for the material dielectric parameters.

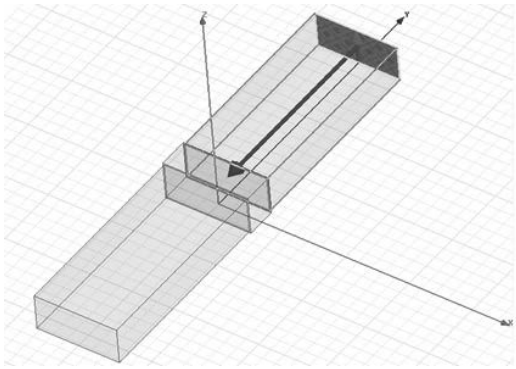

Figure 3.2. Simulation structure in HFSS with de-embedded wave-port excitation [VI].

3.5 Analytical extraction of the material parameters

Various methods, including the classical Nicolson–Ross–Weir (NRW) technique [94–96] and others [92, 97–101], are available for the extraction of the material electromagnetic properties. The basic idea in these methods is to apply the measured (or numerically simulated) reflection and transmission coefficients for the evaluation of the material properties. The intrinsic limitation of the NRW method is related to the electrical thickness of the material sample. In this thesis work, along with the direct comparison of the simulation data sets to the measurement results, dielectric parameters of the test material are also calculated using the modified Nicolson-Ross-Weir (NRW) method [102, 103]. This method can be used to extract the material parameters for the samples thicker than half wavelength and does not require seeking of a solution branch as in the NRW method.

The reflection coefficient in terms of the S-parameters can be written as [94, 95]

$$\Gamma = \chi \pm \sqrt{\chi^2 - 1}, \quad \chi = \frac{S_{11}^2 - S_{21}^2 + 1}{2S_{11}}. \tag{3.4}$$

For the wave propagating through the material sample of thickness d, the phase factor is given by

$$e^{-\gamma d} = \frac{S_{11} + S_{21} - \Gamma}{1 - (S_{11} + S_{21})\Gamma} = e^{-\alpha d} e^{-j(\beta d + 2\pi m)} = A e^{j\phi}, \tag{3.5}$$

where $\gamma = j\omega\sqrt{\mu_0 \varepsilon_0}\sqrt{n^2 - (\omega_c/\omega)^2}$, n is the refractive index, ω is the angular frequency and ω_c is the angular cut-off frequency of the transmission line section, α is the attenuation constant, β is the propagation

constant, and m is an integer. Then, according to [94, 95] the material properties can be extracted using

$$n^2 = \varepsilon_r \mu_r = -\left[\frac{c}{\omega d}\ln(e^{\gamma d})\right]^2 + \left(\frac{\omega_c}{\omega}\right)^2, \tag{3.6}$$

where c is the speed of light (3×10^8 m/s).

The limitation with this approach relates to the periodicity of the phase factor in (3.5) resulting in an infinite number of roots. This complicates the extraction process since one needs to verify the correct root and the correct branch of solution in (3.6) at each measurement point. The modified NRW method [102] addresses this problem by measuring the phase difference between the preceding measurement points. This helps to maintain the correct branch of solution throughout the measurement process. The advantage of this approach is that the verification of the choice of the correct branch is required only at the first measurement point. However, two conditions are required to be fulfilled in order to obtain accurate extraction results applying this method. First, the phase difference between two consecutive measurement points should not exceed π and second, the thickness of the material sample should be less than $\lambda/2$ at the lowest measurement frequency.

The phase factor in terms of the S-parameters and the wave impedance is given as

$$e^{\gamma d} = \frac{1 - S_{11}^2 + S_{21}^2}{2S_{21}} + \frac{2S_{11}}{(z - \frac{1}{z})S_{21}}, \tag{3.7}$$

where

$$z = \sqrt{\frac{(1 + S_{11})^2 - S_{21}^2}{(1 - S_{11})^2 - S_{21}^2}}. \tag{3.8}$$

For N measurement frequency points, the corresponding arguments are given by (3.5) and the argument term at point N can be written as [102]

$$\phi_N = \phi_0 + \sum_{i=1}^{N} \arg\left(\frac{e^{\gamma_i d}}{e^{\gamma_{i-1} d}}\right), \tag{3.9}$$

where ϕ_0 is the phase value at the first measurement point. The natural logarithm of the exponential in (3.6) can be expressed in the following form [102]

$$\ln(e^{\gamma d}) = \ln(\left|e^{\gamma d}\right|) + j \arg(e^{\gamma d}). \tag{3.10}$$

Then, the refractive index of the material is extracted using [102]

$$\sqrt{(n_N^2) - (\omega_c/\omega_N)^2} = \frac{1}{k_0 d}\left[-j\ln\left(\left|e^{\gamma_N d}\right|\right) + \phi_0 + \sum_{i=1}^{N}\arg\left(\frac{e^{\gamma_i d}}{e^{\gamma_{i-1} d}}\right)\right]. \quad (3.11)$$

Finally, the permittivity and the loss tangent of the material sample can be computed with the equations

$$n_N = \sqrt{\varepsilon_r \mu_r}, \quad \text{and} \quad (3.12)$$

$$\tan\delta = \frac{\varepsilon''}{\varepsilon'}. \quad (3.13)$$

3.6 Extraction results

3.6.1 From direct comparison

In the direct comparison, measured reflection and transmission coefficients are compared with the simulation data sets of different permittivity and loss tangent values. The least square error curve fitting method is applied to obtain the best fit of the simulated coefficients to the measured counterparts. For example, in case of a Teflon material sample, a dielectric constant of 2.0 and loss tangent of 0.003 are estimated from the curve fitting of the transmission coefficient phase. For the unknown polymer, the best fit values are found to be 2.4 and 0.06 for the dielectric constant and loss tangent, respectively. Figures 3.3 and 3.4 present the measured and simulated (best fit) transmission coefficient phase plots for both the Teflon and the polymer material.

Here, a $\pm 10\%$ deviation on the dielectric constant of Teflon and a $\pm 12.5\%$ on that of the polymer are simulated and compared with the measured results. It is observed that the measurement data points are within the limits for the whole measurement frequency band indicating that the accuracy of the extraction results, obtained in this particular case, is within $\pm 12.5\%$.

The loss tangent of the material sample is extracted similarly by comparing the measured and simulated loss incurred by the material sample which can be calculated from the S-parameters as

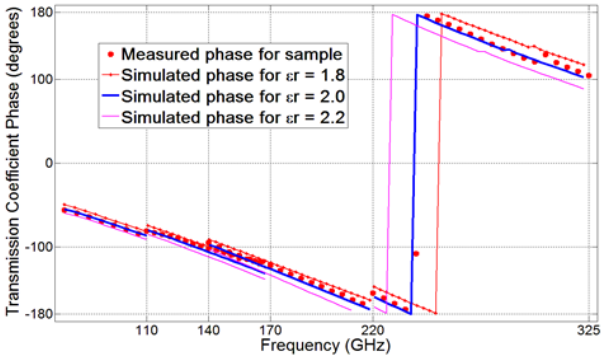

Figure 3.3. Least square curve fitting of the measured transmission coefficient phase for Teflon with $\pm 10\%$ deviation in simulated dielectric constant value [VI].

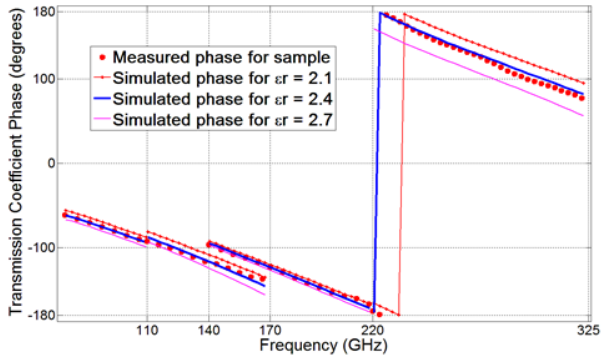

Figure 3.4. Least square curve fitting of the measured transmission coefficient phase for polymer material with $\pm 12.5\%$ deviation in the simulated dielectric constant value [VI].

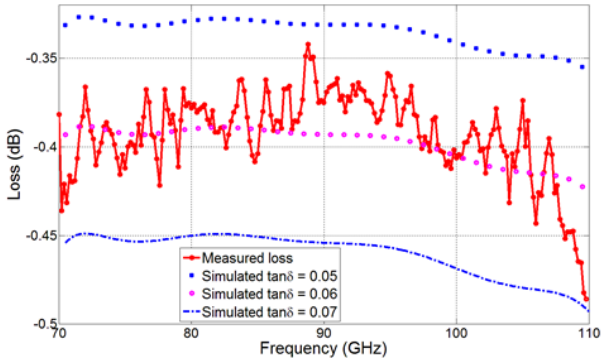

Figure 3.5. Measured loss for unknown polymer compared with the simulated losses for different values of loss tangent [VI].

$$Loss(dB) = -10\log_{10}\left(\left|S_{11}^2\right| + \left|S_{21}^2\right|\right). \tag{3.14}$$

Figure 3.5 shows the loss tangent extraction of the unknown polymer where the losses computed using different simulated loss tangent values

are compared with the measured loss. It is observed that the best fit is obtained for loss tangent value of 0.06. In case of Teflon material, the best value is obtained at 0.003.

3.6.2 From analytical calculations

The least square fitting of the measured data to the simulated ones provides a good estimation of the dielectric properties of the material sample. However, it is important to verify analytically if the estimated parameters are realistic and accurate. As explained in Section 3.5, the permittivity and the loss tangent of the MUTs are computed (in MATLAB) from the measured reflection and transmission coefficients. For the comparison purpose, analytical calculations are also applied to the simulated reflection and transmission coefficients that are found to be the best fits as mentioned in Section 3.6.1.

Figures 3.6 and 3.7 present the analytically computed permittivity and loss tangent for Teflon and for the unknown polymer, respectively, over the frequency range of 75–325 GHz. Extraction of the material parameters are performed using both the measured and simulated S-parameters.

It is observed that the computed values of the permittivity and the loss tangent are in a close agreement with the values that are obtained from direct comparison except some ambiguities in the frequency range from 200 GHz to 250 GHz. The uncertainty in this frequency range is related to the thickness resonance of the material sample. The thickness of the material sample around 230 GHz is one half of the guided wavelength in the material making S_{11} very small and leading to higher uncertainty in the phase and consequently on the extracted parameters. Further, propagation of the higher modes is possible in case of inhomogeneous sample and the presence of air gaps between the sample and waveguide walls. Overmoding problem is even worse while measuring samples with high dielectric constants as the cutoff frequency changes promoting the propagation of higher modes in the waveguide [104]. In this work, the samples with the same thickness have been used. In the future work, different thickness samples could be measured to avoid resonances in the extracted results.

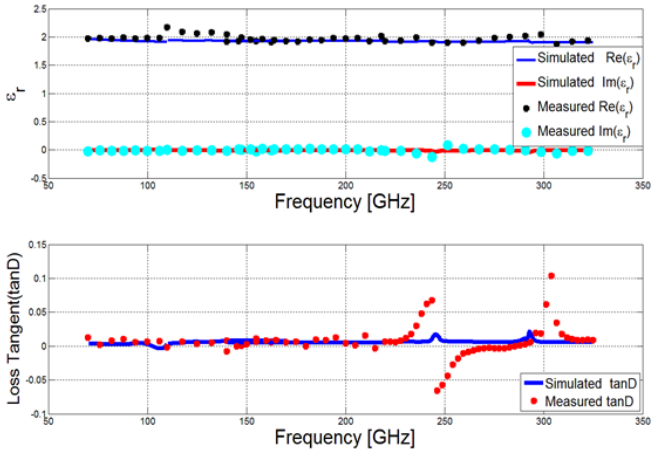

Figure 3.6. Extracted permittivity and loss tangent for Teflon [VI].

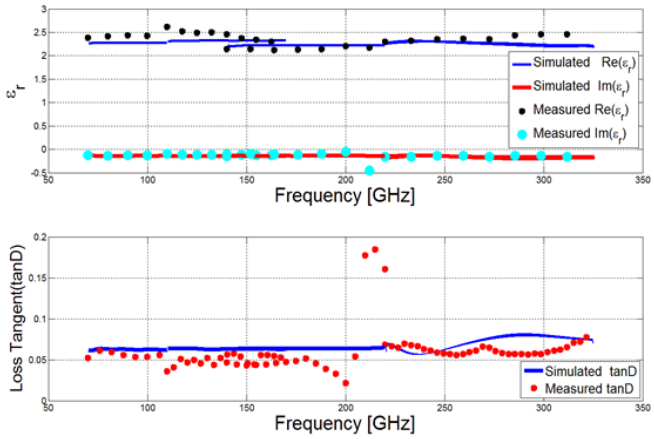

Figure 3.7. Extracted permittivity and loss tangent for unknown polymer [VI].

3.7 Application

The ability to manufacture electronic devices in a large area at a low cost has made printing technology a promising method compared to the printed circuit technology for fabrication of microwave and millimeter wave components on a substrate materials [105, 106]. Other advantages of printed electronics are light weight, flexibility and easy integration.

It is essential to obtain the material properties, such as, permittivity and loss tangent, prior to the design and printing of the electronic structures to the polymer materials. In this thesis work, the method presented in the previous sections is applied to study the dielectric properties of various polymer substrate materials and their suitability for printing millimeter wave components [VII]. Five different materials have been char-

acterised including inexpensive substrates, such as Polyethylene Terephthalate (PET), Polyethylene Naphthalate (PEN), Polymethyl Methacrylate (PMMA) and Polyimide film (PI), and specific plastic material, such as, Preperm255. An example plot of the extracted permittivity and loss tangent for PET material in WR-10 (75-110 GHz) frequency band is shown in Figure 3.8. At 90 GHz, the permittivity of 3.5 and loss tangent of 0.03 are obtained from the extraction.

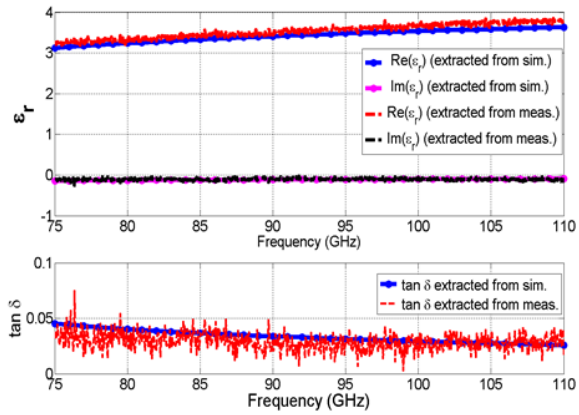

Figure 3.8. Extracted dielectric parameters from measured and simulated S-parameters for PET (Melinex) material sample [VII].

The extracted dielectric parameters of all five materials at 90 GHz are listed in Table 3.1. The Preperm255 material exhibited lower loss compared to other measured materials which makes it a potential candidate for printing the components, such as antennas for millimeter wavelengths. However, a test print on this material, with reverse-offset printing method, indicated the material to be unsuitable as there was no proper ink transfer leading to a bad quality of the printed samples. At least partly this was due to the rougher surface of the Preperm255 material compared to the other tested substrate materials. Further studies and experiments are being made on the evaluation of ink properties (conductivity), achievable conductor thickness, and printing accuracy. Furthermore, printing process is being optimized to obtain better quality printed samples for testing of the millimeter wave components.

Table 3.1. Dielectric parameters for different material extracted from simulation and measurement results at 90 GHz [VII].

Material	ε_r (sim.)	ε_r (meas.)	$tan\delta$ (sim.)	$tan\delta$ (meas.)
PET	3.5	3.4	0.035	0.03
PMMA	2.3	2.3	0.02	0.02
PI	4.0	4.1	0.04	0.04
PEN	3.1	3.2	0.03	0.045
Preperm255	2.5	2.4	0.005	0.004

4. Summary of publications

Publication I: "New verification routine for pulsed I-V and transient current measurement setup applied to a THz Schottky diode"

A verification routine is developed in [I] for validating extremely fast pulsed I-V and transient current measurement setups. The latter one is used in [II] for extracting the thermal parameters of the THz Schottky diodes. The minimum pulse width of 300 ns is found to be feasible for pulsed I-V measurements and the current settling time in transient measurements is found to depend on the level of heating current applied to the DUT.

Publication II: "Thermal characterization of THz Schottky diodes using transient current measurements"

A novel method for extraction of the thermal properties of THz Schottky diodes is introduced in [II] which is based on the transient current measurements. The parameters, such as the thermal resistance, thermal time-constants and peak junction temperatures are extracted for single-anode varactor Schottky diodes with three different anode sizes (5, 9, and $12\,\mu m^2$). The extracted total thermal resistance, for the diode with $9\,\mu m^2$ anode area, is compared with the result from an in-house measurement-based method and with the simulation results from two commercial 3D thermal simulators. For this particular diode, the total thermal resistance is within 10 $\%$ of the average value of 4020 K/W when using all four approaches. The developed method can be applied to characterise small area diodes with the thermal time-constant down to 300 ns.

Publication III: "Characterisation of THz Schottky diodes for MetOp-SG instruments"

An application of the thermal charactersation method developed in [II] is demonstrated in [III]. Schottky-diode based mixer and multiplier prototypes for the MetOp-SG satellite instruments are thermally characterised as a part of the reliability assessment. Five frequency multiplier and two mixer prototype blocks are measured. In addition to the thermal measurements, RF tests are also performed for three identical multiplier prototypes and their comparison illustrate that the prototype with larger thermal resistance (or peak temperature) has smaller output power as well as lower efficiency.

Publication IV: "Experimental investigation of traps in THz Schottky diodes"

In [IV], experimental investigation is made in order to identify the charge trapping in THz Schottky diodes using various measurement techniques, such as I-V, capacitance and low-frequency noise measurement. Presence of traps are indicated in I-V and C-V results. However the effect is observed clearly in capacitance-frequency (C-f) and low-frequency noise measurements.

Publication V: "Characterisation of low-barrier Schottky diodes for millimeter wave mixer applications"

Low-barrier Schottky diodes from ACST GmbH are characterised in [V] in order to study the suitability of such diodes for millimeter wave mixing applications. A test diode is mounted on a fundamental mixer test-jig platform, and conversion loss and noise temperature measurements are carried out. In addition, 3D HFSS and ADS circuit simulations are also performed and the results are presented. Conversion loss of less than 5 dB is obtained for 0.1 mW LO power in mixer operation at 181-183 GHz.

Publication VI: "Measurement of dielectric properties at 75 - 325 GHz using a vector network analyzer and full-wave simulator"

In [VI], an easy-to-use method for determination of dielectric properties of

the material at millimeter wave frequencies (75–325 GHz) is introduced. Dielectric properties of Teflon and an unknown polymer are extracted both by comparing the simulated S-parameters with the measured ones and by solving analytically equations with the measured S-parameters (modified NRW method). The extracted result from both approaches are found to be in close agreement

Publication VII: "Towards printed millimeter-wave components: Material characterization"

An application of the material parameter extraction method introduced in [VI] is presented in [VII], where the dielectric properties of potential substrate materials for printing millimeter wave components, such as antennas, are evaluated. Five different polymer materials are studied and their permittivity and loss tangent are extracted in the frequency range from 75–110 GHz.

5. Discussions, conclusions and future work

The research work presented in this doctoral thesis focuses on the characterisation of Schottky diodes and dielectric materials, both for millimeter and terahertz wave applications. The results of this research work are reported in publications [I]–[VII]. Chapters 1–4 summarize the background and objective of the research work, characterisation methods developed both for THz Schottky diodes and for dielectric materials, and their applications as well as the scientific contributions of the research work.

The first part of the thesis describes the efforts made for characterisation of the Schottky diode in terms if its thermal, noise and RF performances [I]–[V]. The existing and the newly developed characterisation methods are presented to study the Schottky diode characteristics for millimeter wave and THz applications. The second part of the thesis presents the characterisation studies made for extracting dielectric properties of materials at millimeter wave frequencies [VI, VII].

Starting with the first part of the thesis, a novel thermal characterisation method is developed in this work [II]. This method is based on the transient current measurements and is suitable for small area THz Schottky diodes with fast thermal time-constants. The capability of the method to extract all the thermal parameters, i.e, thermal resistance, thermal time-constants and peak junction temperature of the diode is demonstrated. The limitations of the standard characterisation methods, such as electrical transients and self-heating, are addressed by using ultra-fast measurement equipment and small measurement current levels, respectively. Three single anode varactor diodes with different anode sizes are characterised. Furthermore, comparison of the extraction results from the developed method against two 3D commercial simulators and also against an in-house measurement-based method are presented.

Thermal simulations, to observe the temporal response of the diode, can

be performed using commercial simulation tool such as COMSOL Multiphysics that can predict the thermal time-constants of the diode. This facilitates the pre-fabrication process. However, experimental determination is crucial to obtain the realistic thermal performance of the diodes under test. Nevertheless, perdiction of the thermal time-constants with a commercial simulation tool can add an advantage to the developed measurement based thermal characterisation method and will be explored as a future work.

The thermal characterisation method in this work applies DC voltage source to heat the diode and then measure the current response as the diode cools down. Using an RF signal to heat the diode and measure its thermal performance would have added an advantage to this method. However, the RF signal cannot be switched on and off quickly enough for obtaining meaningful measurement results. Further, applying an RF signal will change the I-V operating point of the diode resulting in inaccurate measurements.

The new characterisation method developed in this work is applied to thermally test the Schottky-diode based mixer and multiplier prototype blocks for the MetOp-SG satellite instruments as a part of the reliability assessment. These thermal tests provide the operating peak junction temperatures and the heat flow (thermal time-constants) in the Schottky diodes which is a vital information regarding the reliability of the satellite instruments. In addition, comparisons of the thermal characterisation results are made with the RF results of three identical multiplier blocks. It is illustrated that the block with higher thermal impedance has lower output power as well as lower efficiency. Hence, some interrelation between the thermal and RF measurement results are observed. Furthermore, it is noted that the thermal characterisation method can be a good tool for checking the reproducibility of the assembly of discrete devices. For the multiplier blocks with multiple anodes, the measured peak temperature is an effective temperature of all the anodes since each individual anode temperature cannot be determined with the presented measurement setup. However, with the help of a simulation tool this difference in anode temperature can be predicted and is considered as a future extension to this work.

The accuracy and consequently the reliability of the extraction results from the developed thermal characterisation method in [II] is determined by the accuracy of the measurement system. Hence, a verification rou-

tine is required, before the characterisation procedure, to ensure that the diode parameter space is within the verified range during the measurements. Such a verification routine is developed in [I] for validating the extremely fast pulsed I-V and transient current measurement setups. The measurements performed for the routine include pulsed I-V measurements with different pulse widths (using several voltage and current levels) as well as transient current measurements using different heating and measurement current levels. It is found that the minimum usable pulse width in the presented measurement setup is 300 ns and the current settling time is determined by the applied heating current level.

As a continuation of the Schottky diode characterisation work, experimental investigations on the charge trapping and low-frequency noise in THz Schottky diodes are made in this thesis work [IV]. Evidence of the presence of traps is observed using various measurement techniques including I-V, capacitance and low-frequency noise measurements. Among the applied measurement methods, the low-frequency noise measurement method is found to be the most suitable for identifying and characterising charge trapping in THz Schottky diodes. As a future work, a quantitative study and analysis is to be performed to improve the understanding of trapping effects and their origin in small area THz Schottky diodes.

Further, a study on suitability of the low-barrier Schottky diode for millimeter wave mixer applications is performed [V]. The low-barrier height enables a lower LO power requirement in the mixer operation. Hence, it is desirable to obtain a low-barrier Schottky-diode mixer that can operate at low LO power but has an acceptable conversion loss and noise temperature. In this work, such a low-barrier diode from ACST GmbH is characterised for its performance in a mixing operation at millimeter wave frequencies. The conversion loss and noise temperature are evaluated both from measurements and simulations and the results are presented. It is observed that with a low-barrier Schottky diode, the LO power can be significantly reduced while maintaining acceptable conversion loss and noise temperature. The actual noise model, valid for the low-power detector design, is found to be invalid when designing low-power mixers. Hence, the noise model is modified and simulations are performed. It is illustrated that with the new noise model the results are promising. However, as a future work, these results are to be verified with measurements of the diodes .

Study of the material properties at millimeter wave frequencies both

with measurements and simulations is performed in the second part of this research work. Various methods are available for extraction of the material parameters. However, each method has its own advantages and limitations depending on the MUT and the measurement condition. The transmission line technique can be applied for an easy, non-destructive and wideband material parameter extraction at millimeter wave frequencies. In this work, an easy-to-use method, based on the transmission line method, for determination of dielectric properties of the material at millimeter wave frequencies (75–325 GHz) is presented [VI]. Material's dielectric properties are extracted using two approaches. First, by comparing the simulated S-parameters with the measured ones, and second, by solving analytical equations with the measured S-parameters (modified NRW method). The application of the developed method is presented in [VII] where an evaluation of the dielectric properties of potential substrate materials for printing millimeter wave components, such as antennas, is performed. Permittivity and loss tangent for five different polymer materials are extracted in the frequency range from 75-110 GHz.

References

[1] P. H. Siegel, "Terhertz technology," *IEEE Transactions on Microwave Theory and Techniques*, vol. 50, no. 3, pp. 910–928, March 2002.

[2] J. H. Wiltse, "History of millimeter and submillimeter waves," *IEEE Transactions on Microwave Theory and Techniques*, vol. 32, no. 9, pp. 1118–1126, September 1984.

[3] T. W. Crowe, W. L. Bishop, D. W. Porterfield, J. L. Hesler, and R. M. Weikle, "Opening the terahertz window with integrated diode circuits," *IEEE Journal of Solid-State Circuits*, vol. 40, no. 10, pp. 2104–2110, October 2005.

[4] P. H. Siegel, "THz instruments for space," *IEEE Transactions on Microwave Theory and Techniques*, vol. 55, no. 11, pp. 2957–2965, November 2007.

[5] J. W. Walters *et al.*, "The earth observation system microwave limb sounder (EOS MLS) in the AURA satellite," *IEEE Transactions on Geoscience and Remote Sensing*, vol. 44, no. 5, pp. 1075–1092, May 2006.

[6] T. Kleine-Ostmann and T. Nagatsuma, "A review on terahertz communications research," *Journal of Infrared, Millimeter and Terahertz Waves*, vol. 32, no. 2, pp. 143–171, January 2011.

[7] W. Menzel, "Millimeter-wave radar for civil applications," in *Proceedings of the 7th European Radar Conference*, Paris, France, September 2010, pp. 261–264.

[8] J. F. Federici, B. Schulkin, F. Huang, D. Gary, R. Barat, F. Oliveira, and D. Zimdars, "THz imaging and sensing for security applications—explosives, weapons and drugs," *Journal of Semiconductor Science and Technology*, vol. 20, no. 7, pp. 266–280, June 2005.

[9] R. Appleby and R. N. Anderton, "Millimeter-wave and submillimeter-wave imaging for security and surveillance," *Proceedings of the IEEE*, vol. 95, no. 8, pp. 1683–1690, August 2007.

[10] S. Wietzke, C. Jansen, M. Reuter, T. Jung, D. Kraft, S. Chatterjee, B. Fischer, and M. Koch, "Terahertz spectroscopy on polymers: A review of morphological studies," *Journal of Molecular Structure*, vol. 1006, pp. 41–51, 2011.

[11] P. H. Siegel, "Terahertz technology in biology and medicine," *IEEE Transactions on Microwave Theory and Techniques*, vol. 52, no. 10, pp. 2438–2447, October 2004.

[12] G. Chattopadhyay, "Technology, capabilities, and performance of low power terahertz sources," *IEEE Transactions on Terahertz Science and Technology*, vol. 1, no. 1, pp. 33–53, September 2011.

[13] T. W. Crowe, R. J. Mattauch, H. P. Roser, W. L. Bishop, W. C. B. Peatman, and X. Liu, "GaAs Schottky diodes for THz mixing applications," *Proceedings of the IEEE*, vol. 80, no. 11, pp. 1827–1841, November 1992.

[14] M. Hoefle, K. Haehnsen, I. Oprea, O. Cojocari, A. Penirschke, and R. Jakoby, "Highly responsive planar millimeter wave zero-bias Schottky detector with impedance matched folded dipole antenna," in *IEEE MTT-S International Microwave Symposium*, Seattle, WA, USA, 2013.

[15] S. A. Maas, *Nonlinear Microwave and RF Circuits*. Norwood, MA, USA: Artech House Inc., 2003.

[16] S. Maas, *Microwave Mixers*. Norwood, MA, USA: Artech House Inc., 2002.

[17] D. Young and J. Irvin, "Millimeter frequency conversion using Au-ntype GaAs Schottky barrier epitaxial diodes with a novel contacting technique," *Proceedings of the IEEE*, vol. 53, no. 12, pp. 2130–2131, December 1965.

[18] T. Nozokido, J. Chang, C. Mann, T. Suzuki, and K. Mizuno, "Optimization of a Schottky barrier mixer diode in the submillimeter wave region," *International Journal of Infrared and Millimeter Waves*, vol. 15, pp. 1851–1865, November 1994.

[19] A. Betz and R. Boreiko, "A practical Schottky mixer for 5 THz (Part II)," in *Proceedings of the 7th International Symposium on Space Terahertz Technology*, Charlottesville, VA, USA, March 1996, pp. 503–510.

[20] W. Bishop, K. McKinney, R. Mattauch, T. Crowe, and G. Green, "A novel whiskerless Schottky diode for millimeter and submillimeter wave application," in *IEEE MTT-S International Microwave Symposium Digest*, vol. 2, Palo Alto, CA, USA, 1987, pp. 607–610.

[21] W. Bishop, E. Meiburg, R. Mattauch, T. Crowe, and L. Poli, "A micron-thickness, planar Schottky diode chip for terahertz applications with theoretical minimum parasitic capacitance," in *IEEE MTT-S International Microwave Symposium Digest*, vol. 3, Dallas, TX, USA, May 1990, pp. 1305–1308.

[22] P. H. Ostdiek, "Integration of anti-parallel pair of planar Schottky barrier diodes for millimeter and submillimeter wavelengths," Ph.D. dissertation, School of Engineering and Applied Science, University of Virginia, Charlottesville, USA, 1991.

[23] A. Maestrini, I. Mehdi, R. Lin, J. V. Siles, C. Lee, J. Gill, G. Chattopadhyay, E. Schlecht, B. Thomas, and J. Ward, "A 2.5-2.7 THz room temperature electronic source," in *22nd International Symposium on Space Terahertz Technology*, Tucson, Arizona, April 2011, pp. 1–4.

[24] A. Y. Tang, "Modelling of terahertz planar Schottky diodes," Ph.D. dissertation, Chalmers University of Technology, Goeteborg, Sweden, 2011.

[25] S. Montanari, "Fabrication and characterization of planar Gunn diodes for monolithic microwave integrated circuits," Ph.D. dissertation, RWTH, Aachen, Germany, 2005.

[26] S. M. Sze and K. K. Ng, *Physics of Semiconductor Devices*. Hoboken, NJ, USA: John Wiley and Sons Inc., 2007.

[27] M. Shur, *GaAs Devices and Circuits*. New York, NY, USA: Plenum Press, 1987.

[28] M. T. Faber, J. Chramiec, and M. E. Adamski, *Microwave and Millimeter-Wave Diode Frequency Multipliers*. Norwood, MA, USA: Artech House Inc., 1995.

[29] M. Faber, J. Chramiec, and M. E. Adamski, "Semiconductor m-n-n+ diodes for frequency conversion at millimeter and submillimeter waves," *Kwartalnik Elektroniki I Telekomunikacji*, vol. 41, pp. 203–255, 1995.

[30] J. W. Sofia. (1995) Fundamentals of thermal resistance measurement. [Online]. Available: http://samunet.hu/extfil/Temperature_saturation_voltage.pdf

[31] D. L. Blackburn, "Temperature measurements of semiconductor devices - a review," in *20th Annual IEEE Semiconductor Thermal Measurement and Management Symposium*, San Jose, CA, USA, March 2004, pp. 70–80.

[32] A. Y. Tang, E. Schlecht, G. Chattopadhyay, R. Lin, C. Lee, J. Gill, I. Mehdi, and J. Stake, "Steady-state and transient thermal analysis of high-power planar Schottky diodes," in *22nd International Symposium on Space Terahertz Technology*, Tucson, AZ, USA, April 2011.

[33] A. Y. Tang, E. Schlech, R. Lin, G. Chattopadhyay, C. Lee, J. Gill, I. Mehdi, and J. Stake, "Electro-thermal model for multi-anode Schottky diode multipliers," *IEEE Transactions on Terahertz Science and Technology*, vol. 2, no. 3, pp. 290–298, May 2012.

[34] M. A. Saber, "Thermal characterization of THz planar Schottky diodes using simulations," Master's thesis, Aalto University, Aalto, Finland, 2012.

[35] J. Christofferson and A. Shakouri, "Through the substrate, backside thermal measurements on active semiconductor devices using near IR thermoreflectance," in *Proc. 19th Annu. IEEE Semicond. Thermal Meas. Manag. Symp.*, March 11-13 2003, pp. 271–275.

[36] K. Azar, J. R. Benson, and V. P. Manno, "Liquid crystal imaging for temperature measurement of electronic devices," in *Proc. 7th Annu. IEEE Semicond. Thermal Meas. Manag. Symp.*, February 12-14 1991, pp. 23–33.

[37] "Test method for semiconductor devices," U. S. Deptartment of Defense, Tech. Rep. MIL-STD-750E, November 2006.

[38] T. Kiuru, J. Mallat, A. V. Räisänen, and T. Närhi, "Schottky diode series resistance and thermal resistance extraction from S-parameter and temperature controlled measurements," *IEEE Transactions on Microwave Theory and Techniques*, vol. 59, no. 8, pp. 2108–2116, August 2011.

[39] (2013) Agilent B1500A semiconductor device analyzer. [Online]. Available: http://cp.literature.agilent.com/litweb/pdf/B1500-90000.pdf

[40] (2011) Semiconductor characterization system technical data. [Online]. Available: http://www.tek.com/keithley-semiconductor-test-systems

[41] C. Ciofi and B. Neri, "Low-frequency noise measurements as a characterization tool for degradation phenomena in solid-state devices," *Journal of Applied Physics*, vol. 33, pp. 199–216, 2000.

[42] S. Mohammadi, D. Pavlidis, and B. Bayraktaroglu, "Relation between low-frequency noise and long-term reliability of single AlGaAs/GaAs power HBT's," *IEEE Trans. on Electron Devices*, vol. 47, no. 4, pp. 677–686, 2000.

[43] K. B. Cooper and R. J. Dengler, "Residual phase noise and transmit/receive isolation in a submillimeter-wave FMCW radar," in *IEEE MTT-S International Microwave Symposium (IMS2014)*, Tampa, FL, USA, June 2014, pp. 1–4.

[44] J. L. Hesler and T. W. Crowe, "Responsivity and noise measurements of zero-bias Schottky diode detectors," in *Proc. of 18th Int. Symp. on Space Terahertz Technology*, Pasadena, USA, March 2007, pp. 89–92.

[45] T. Tokumitsu, M. Kubota, K. Sakai, and T. Kawai, "Application of GaAs device technology to millimeter-waves," *SEI Technical Review*, no. 79, pp. 57–65, 2014.

[46] H. L. Hartnagel, R. Katilius, and A. Matulionis, *Microwave Noise in Semiconcuductor Devices*. New York, USA: 1st ed., Wiley, 2001.

[47] S. M. Sze, *Physics of Semiconductor Devices*. New York, USA: 2nd ed., Wiley, 1981.

[48] M. Hudait and S. Krupanidhi, "Interface states density distribution in Au/n-GaAs Schottky diodes on n-Ge and n-GaAs substrates," *Materials Science and Engineering B*, vol. 87, pp. 141–147, June 2001.

[49] S. Karatas and S. Altindal, "Temperature dependence of barrier heights of Au/n-type GaAs Schottky diodes," *Solid-State Electronics*, vol. 49, pp. 1052–1054, June 2005.

[50] I. Hussain, M. Y. Soomro, N. Bano, O. Nur, and M. Willander, "Systematic study of interface trap and barrier inhomogeneities using I-V-T characteristics of Au/ZnO nanorods Schottky diode," *Journal of Applied Physics*, vol. 113, p. 234509, June 2013.

[51] K. R. Peta, B. G. Park, S. Lee, M. D. Kim, J. E. Oh, T. G. Kim, and V. R. Reddy, "Analysis of electrical properties and deep level defects in undoped GaN Schottky barrier diode," *Thin Solid Films*, vol. 534, pp. 603–608, February 2013.

[52] I. Hussain, M. Y. Soomro, N. Bano, O. Nur, and M. Willander, "Interface trap characterization and electrical properties of Au-ZnO nanorod Schottky diodes by conductance and capacitance methods," *Journal of Applied Physics*, vol. 112, p. 064506, September 2012.

[53] E. Arslan, S. Butun, Y. Safak, H. Cakmak, H. Yu, and E. Ozbay, "Current transport mechanisms and trap state investigations in (Ni/Au)–AlN/GaN Schottky barrier diodes," *Microelectronics Reliability*, vol. 51, pp. 576–580, October 2010.

[54] M. Jun, M. Jang, Y. Kim, C. Choi, T. Kim, B. Park, and S. Lee, "Analysis of interface trap states at Schottky diode by using equivalent circuit modeling," *Journal of Vacuum Science and Technology B*, vol. 25, pp. 82–85, January 2007.

[55] D. V. Lang, "Deep-level transient spectroscopy: A new method to characterize traps in semiconductors," *Journal of Applied Physics*, vol. 45, pp. 3023–3032, July 1974.

[56] G. Miller, J. Ramirez, and D. Robinson, "A correlation method for semiconductor transient signal measurements," *Journal of Applied Physics*, vol. 46, pp. 2638–2644, June 1975.

[57] G. Miller, D. Lang, and L. Kimerling, "A correlation method for semiconductor transient signal measurements," *Annual Review of Material Science*, vol. 7, pp. 377–448, August 1977.

[58] M. Li and C. Sah, "A new method for the determination of dopant and trap concentration profiles in semiconductors," *IEEE Transactions on Electron Devices*, vol. 29, pp. 306–315, February 1982.

[59] N. Johnson, "Measurement of semiconductor-insulator interface states by constant-capacitance deep-level transient spectroscopy," *Journal of Vacuum Science and Technology*, vol. 21, pp. 303–314, July 1982.

[60] L. Dobaczewski, A. R. Peaker, and K. B. Nielsen, "Laplace-transform deep-level spectroscopy: The technique and its applications to the study of point defects in semiconductors," *Journal of Applied Physics*, vol. 96, pp. 4689–4728, November 2004.

[61] H. P. Gislason and D. Seghier, "Investigation of deep defects using generation-recombination noise," *Optica Applicata*, vol. 36, no. 2, pp. 359–371, 2006.

[62] G. Hartler, U. Golze, and K. Paschke, "Extended noise analysis — A novel tool for reliability screening," *Microelectronics Reliability*, vol. 39, pp. 1193–1198, 1998.

[63] S. Hsu, "Flicker noise in metal semiconductor Schottky barrier diodes due to multistep tunneling process," *IEEE Transactions on Electron Devices*, vol. 18, no. 10, pp. 882–887, October 1971.

[64] T. G. M. Kleinpenning, "Low-frequency noise in Schottky barrier diodes," *IEEE Transactions on Electron Devices*, vol. 22, no. 2, pp. 121–128, February 1979.

[65] S. Hsu, "Low-frequency excess noise in metal–silicon Schottky barrier diodes," *IEEE Transactions on Electron Devices*, vol. 17, no. 7, pp. 496–506, July 1970.

[66] M. Y. Luo, G. Bosman, A. V. D. Ziel, and L. L. Hench, "Theory and experiments of 1/f noise in Schottky-barrier diodes operating in the thermionic-emission mode," *IEEE Transactions on Electron Devices*, vol. 35, pp. 1351–1356, 1988.

[67] J. Lee, J. Brini, G. Kamarinos, C. Dimitriadis, S. Logothetidis, and P. Patsalas, "Low frequency noise measurements on TiN/n-Si Schottky diodes," *Applied Surface Science*, vol. 142, pp. 390–393, 1999.

[68] J. Lee, J. Brini, A. Chovet, and C. Dimitriadis, "Flicker noise by random walk of electrons at the interface in nonideal Schottky diodes," *Solid-State Electronics*, vol. 43, pp. 2185–2189, July 1999.

[69] J. I. Lee and I. K. Han, "Low frequency noise spectroscopy for Schottky contacts," *Journal of the Korean Physical Society*, vol. 37, no. 6, pp. 966–970, December 2000.

[70] R. Singh and D. Kanjilal, "Temperature dependence of 1/f noise in Pd/n-GaAs Schottky barrier diode," *Journal of Applied Physics*, vol. 91, no. 1, pp. 411–413, January 2002.

[71] J. D. Song, W. J. Choi, I. K. Han, and J. I. Lee, "Characteristics of 1/f noise in Au/GaAs Schottky diode embedded with self-assembled InAs quantum dots," *Journal of the Korean Physical Society*, vol. 45, pp. 542–546, December 2004.

[72] M. Hoefle, A. Penirschke, O. Cojocari, A. Amrhein, T. Decoopman, P. Piironen, and R. Jakoby, "1/f-noise prediction in millimeter wave detectors based on quasi vertical Schottky diodes," in *38th International Conference on Infrared, Millimeter, and Terahertz Waves (IRMMW-THz)*, Mainz, Germany, September 2013.

[73] I. Oprea, A. Walber, O. Cojocari, H. Gibson, R. Zimmermann, and H. L. Hartnagel, "183 GHz mixer on InGaAs Schottky diodes," in *21st International Symposium on Space Terahertz Technology*, Oxford, United Kingdom, March 2010.

[74] I. Oprea, O. Cojocari, A. Walber, H. Gibson, R. Zimmermann, and H. L. Hartnagel, "A 183 GHz mixer with low LO power requirements using InGaAs Schottky diodes," in *Proceedings of the WOCSDICE 2010*, Seeheim, 16-19 May 2010.

[75] K. Dahlberg, "Development of on-wafer calibration methods and planar Schottky diode characterisation at THz frequencies," Ph.D. dissertation, School of Electrical Engineering, Aalto University, Espoo, Finland, 2014.

[76] A. V. Räisänen, "Experimental studies on cooled millimeter wave mixers," *Acta Polytechnica Scandinavica, Electrical Engineering Series*, no. 46, 1980. [Online]. Available: http://lib.tkk.fi/Diss/198X/isbn9512283727/

[77] R. Trambarulo and H. S. Berger, "Conversion loss and noise temperature of mixers from noise measurements," *IEEE MTT-S International Microwave Symposium Digest*, pp. 364–365, May 31-June 3 1980.

[78] E. C. Burdette, F. L. Cain, and J. Seals, "In vivo probe measurement technique for determining dielectric properties at VHF through microwave

frequencies," *IEEE Transactions on Microwave Theory and Techniques*, vol. 28, no. 4, pp. 414–427, 1980.

[79] S. Gabriel, R. W. Lau, and C. Gabriel, "The dielectric properties of biological tissues: II. Measurements in the frequency range 10 Hz to 20 GHz," *Physics in Medicine and Biology*, vol. 41, no. 11, p. 2251, 1996.

[80] B. Schulte *et al.*, "60 GHz WLAN applications and implementation aspects," *EuMA International Journal of Microwave and Wireless Technologies*, vol. 3, no. 2, pp. 213–221, April 2011.

[81] J. Hasch, E. Topak, R. Schnabel, T. Zwick, R. Weigel, and C. Waldschmidt, "Millimeter-wave technology for automotive radar sensors in the 77 GHz frequency band," *IEEE Transactions on Microwave Theory and Techniques*, vol. 60, no. 3, pp. 845–860, March 2012.

[82] X. Wang and A. Stelzer, "A 79 GHz LTCC RF-frontend for short range applications," in *IEEE MTT-S International Microwave Symposium Digest*, June 2011, pp. 1–4.

[83] K. K. Jung, S. W. Yoon, Y. S. Chae, and J. K. Rhee, "Development of a passive millimeter-wave imaging system," in *Proceedings of International Waveform Diversity and Design Conference*, February 2009, pp. 188–191.

[84] J. D. Kraus, *Electromagnetics*, 3rd ed. New York, NY, USA: McGraw-Hill, 1987.

[85] D. K. Cheng, *Fields and Wave Electromagnetics*, 2nd ed. Reading, MA, USA: Addison – Wesley, 1989.

[86] J. B. Jarvis, M. D. Janezic, B. F. Riddle, P. Kabos, C. L. Holloway, R. G. Geyer, and C. A. Grosvenor, "Measuring the permittivity and permeability of lossy materials: Solids, liquids, metal, building materials, and negative-index materials," National Institute of Standards and Technology, Tech. Rep. 1536, February 2005. [Online]. Available: http://nvlpubs.nist.gov/nistpubs/Legacy/TN/nbstechnicalnote1536.pdf

[87] D. K. Ghodgaonkar, V. V. Varadan, and V. K. Varadan, "A free-space method for measurement of dielectric constants and loss tangents at microwave frequencies," *IEEE Transactions on Instrumentation and Measurement*, vol. 38, no. 3, pp. 789–793, June 1989.

[88] J. C. A. Santos, M. H. C. Dias, A. P. Aguiar, I. B. Jr, and L. E. P. Borges, "Using the coaxial probe method for permittivity measurements of liquids at high temperatures," *Journal of Microwaves, Optoelectronics and Electromagnetic Applications*, vol. 8, no. 1, pp. 78–91, June 2009.

[89] E. Kilic, U. Siart, O. Wiedenmann, U. Faz, R. Ramakrishnan, P. Saal, and T. F. Eibert, "Cavity resonator measurement of dielectric materials accounting for wall losses and a filling hole," *IEEE Transactions on Instrumentation and Measurement*, vol. 62, no. 2, pp. 401–407, February 2013.

[90] J. Sheen, "A dielectric resonator method of measuring dielectric properties of low loss materials in the microwave region," *Measurement Science and Technology*, vol. 19, pp. 1–11, April 2008.

[91] W. B. Weir, "Automatic measurement of complex dielectric constant and permeability at microwave frequencies," *Proceedings of IEEE*, vol. 62, pp. 33–36, November 1970.

[92] J. B. Jarvis, E. J. Vanzura, and W. A. Kissck, "Improved technique for determining complex permittivity with transmission/reflection method," *IEEE Transactions on Microwave Theory and Techniques*, vol. 38, pp. 1096–1103, August 1990.

[93] M. S. Venkatesh and G. S. V. Raghavan, "An overview of dielectric properties measuring techniques," *Canadian Biosystems Engineering*, vol. 47, pp. 7.15–7.30, 2005.

[94] A. M. Nicolson and G. F. Ross, "Measurement of the intrinsic properties of materials by time-domain techniques," *IEEE Transactions on Instrumentation and Measurement*, vol. 19, no. 4, pp. 377–382, November 1970.

[95] W. B. Weir, "Automatic measurement of complex dielectric constant and permeability at microwave frequencies," *Proceedings of the IEEE*, vol. 62, no. 1, pp. 33–36, January 1974.

[96] T. L. Blakney and W. B. Weir, "Comments on 'automatic measurement of complex dielectric constant and permeability at microwave frequencies," *Proceedings of the IEEE*, vol. 63, no. 1, pp. 203–205, January 1975.

[97] W. Barry, "A broad-band, automated, stripline technique for the simultaneous measurement of complex permittivity and permeability," *IEEE Transactions on Microwave Theory and Techniques*, vol. 34, no. 1, pp. 80–84, January 1986.

[98] D. R. Smith, S. Shultz, P. Markos, and C. M. Soukoulis, "Determination of effective permittivity and permeability of metamaterials from reflection and transmission coefficients," *Physical Review B*, vol. 65, p. 195104, 2002.

[99] X. Chen, T. M. Grzegorczyk, B.-I. Wu, J. Pacheco, and J. A. Kong, "Robust method to retrieve the constitutive effective parameters of metamaterials," *Physical Review E*, vol. 70, p. 016608, 2004.

[100] D. R. Smith, D. C. Vier, T. Koschny, and C. M. Soukoulis, "Electromagnetic parameter retrieval from inhomogeneous metamaterials," *Physical Review E*, vol. 71, p. 036617, 2005.

[101] V. V. Varadan and R. Ro, "Unique retrieval of complex permittivity and permeability of dispersive materials from reflection and transmitted fields by enforcing causality," *IEEE Transactions on Microwave Theory and Techniques*, vol. 55, no. 10, pp. 2224–2230, October 2007.

[102] O. Luukkonen, S. I. Maslovski, and S. A. Tretyakov, "A stepwise Nicolson–Ross–Weir-based material parameter extraction," *IEEE Antennas and Wireless Propagation Letters*, vol. 10, pp. 1295–1298, November 2011.

[103] A. L. de Paula, M. C. Rezende, and J. J. Barroso, "Modified Nicolson–Ross–Weir (NRW) method to retrieve the constitutive parameters of low-loss materials," in *IEEE MTT-S International Microwave Optoelectronics Conference (IMOC)*, October 2011, pp. 488–492.

[104] J. B. Jarvis, M. D. Janezic, J. H. Grosvenor, and R. G. Geyer, "Transmission/Reflection and Short-Circuit Line Method for Measuring the permittivity and permeability," National Institute of Standards and Technology, Tech. Rep. 1355, May 1992. [Online]. Available: http://nvlpubs.nist.gov/nistpubs/Legacy/TN/nbstechnicalnote1355.pdf

[105] G. Orecchini, R. Zhang, J. Agar, D. Staiculescu, M. M. Tentzeris, L. Roselli, and C. P. Wong, "Inkjet printed organic transistors for sustainable electronics," in *60th IEEE Electronic Components and Technology Conference (ECTC)*, Las Vegas, USA, June 2010.

[106] A. Bisognin, C. Luxey, D. Titz, F. Ferrero, J. Thilleux, W. Wei, H. Happy, and P. Brachat, "Antenna on PEN substrate for millimeter-wave applications," in *IEEE International Symposium on Antennas and Propagation*, Orlando, USA, July 2013, pp. 684–685.

Errata

Publication VI

In equation (2) of Section 6, the summation term should read as,
$\sum_{i=1}^{N} \arg\left(\frac{e^{\gamma_i d}}{e^{\gamma_{i-1} d}}\right)$

Aalto-DD 37/2017

ISBN 978-952-60-7318-7 (printed)
ISBN 978-952-60-7317-0 (pdf)
ISSN-L 1799-4934
ISSN 1799-4934 (printed)
ISSN 1799-4942 (pdf)

Aalto University
School of Electrical Engineering
Department of Electronics and Nanoengineering
www.aalto.fi

BUSINESS + ECONOMY

ART + DESIGN + ARCHITECTURE

SCIENCE + TECHNOLOGY

CROSSOVER

DOCTORAL DISSERTATIONS